

This is an Open Access document downloaded from ORCA, Cardiff University's institutional repository: <https://orca.cardiff.ac.uk/id/eprint/133174/>

This is the author's version of a work that was submitted to / accepted for publication.

Citation for final published version:

Wu, Zhangming , Li, Hao and Chen, Yuli 2020. An improved model for unsymmetric plates. *Composite Structures* 252 , 112622. 10.1016/j.compstruct.2020.112622

Publishers page: <https://doi.org/10.1016/j.compstruct.2020.112622>

Please note:

Changes made as a result of publishing processes such as copy-editing, formatting and page numbers may not be reflected in this version. For the definitive version of this publication, please refer to the published source. You are advised to consult the publisher's version if you wish to cite this paper.

This version is being made available in accordance with publisher policies. See <http://orca.cf.ac.uk/policies.html> for usage policies. Copyright and moral rights for publications made available in ORCA are retained by the copyright holders.



An improved model for unsymmetric plates

Zhangming Wu^{a,c}, Hao Li^b, Yuli Chen^d

^a*Key Laboratory of Impact and Safety Engineering, Ministry of Education of China, Ningbo University, Ningbo, 315211, China.*

^b*Shanghai Institute of Satellite Engineering, P.R. China*

^c*Cardiff School of Engineering, Queens Buildings, The Parade, Newport Road, Cardiff CF24 3AA, UK*

^d*Institute of Solid Mechanics, Beihang University, Beijing 100191, China*

Abstract

For an unsymmetric plate, a pure bending (plate curvature) inevitably causes a certain amount of stretching to the geometric mid-plane due to the stretching-bending coupling. However, in the classical thin plate theory, the geometric mid-plane is assumed to remain unstrained under a pure bending. In this study, we demonstrate that the classical thin plate theory based on Kirchhoff-Love hypothesis is not accurate to model the structural behavior of unsymmetric plates. To overcome this limitation, we propose an improved theoretical model for unsymmetric plates through taking advantages of neutral plane strains in defining the geometric functions instead of mid-plane strains. Subsequently, the new governing equations and energy expression for the cylindrical bending of unsymmetric plates are derived using a modified constitutive equation. An alternative derivation approach based on the general stress equations is also presented for further validation. A direct consideration of stretching-bending coupling in the constitutive equation can significantly reduce the number of unknown parameters in establishing an accurate analytical model for unsymmetric plates. The pure bending problem of unsymmetric plates with small deformation is first studied, for which the improved model proposed in this paper is shown to capture the out-of-plane deformation of unsymmetric plates, accurately. However, many previous works have to take into account the nonlinear von Kármán strains even in the

*Corresponding author

Email address: wuzhangming@nbu.edu.cn; wuz12@cardiff.ac.uk (Zhangming Wu)

model of this small deformation problem. For the pure plate bending problem with large deformation, few unknown terms are needed for the improved model to give accurate results compared with the conventional mid-plane strain based method. Later, this improved model is applied to predict the stable configurations, the bifurcation/loss-of-bifurcation and the static snap-through phenomena of bistable cross-ply composite laminates. Furthermore, the application of this improved model for the accurate simulation of the nonlinear dynamics of unsymmetric plates is also demonstrated. Applying this proposed improved model, the model is reduced into an analogous one for isotropic or symmetric plates, therefore, the problem of unsymmetric plates can be solved readily and accurately.

Keywords: unsymmetric plates, compatibility equation, mid-plane strains membrane strains, Rayleigh-Ritz method

1. Introduction

The classical Kirchhoff–Love thin plate theory is based on the following assumptions: thickness is much smaller than the other physical dimensions; deflections are small compared to the plate thickness; normals remain perpendicular to the mid-plane before and after deformation; mid-plane remains unstrained during bending [1, 2]. Because the material anisotropy is not taken into consideration in the Kirchhoff-Love theory of plates, the mid-plane coincides with the neutral plane after bending.

In the study of mechanics of composite structures, the Kirchhoff-Love theory is often applied to model thin composite plates and shells. In the Kirchhoff-Love theory of plates, the mid-plane of a composite plate is assumed to be unstrained under pure bending [3]. However, for an unsymmetric plate, the mid-plane does not always coincide with the neutral plane. Due to the stretching-bending coupling, a pure bending will introduce in-plane strains to the mid-plane of an unsymmetric plate, and vice versa. Therefore, this phenomenon is in conflict with the assumption of thin plate theory that the mid-plane remains unstrained during the pure bending. Many researchers realized that the linear classical thin plate theory is not accurate for the analysis of unsymmetric plates [4, 5, 6], the mid-plane strain conflict or early bending-extension coupling is not considered in their studies. As an alternative, the large deformation plate theory based on von Kármán nonlinear strains was often employed even for "small deformation analysis"

of unsymmetric laminates [4, 5, 6, 7, 8]. For example, in the study of unsymmetric composite plates that were cooling down from the curing temperature, the Kirchhoff-Love thin plate theory is applied to establish the Rayleigh-Ritz model to predict their deformed shapes. In this method, the mid-plane strains are directly expanded into polynomials, and analytical solutions are obtained through minimizing the potential energy of unsymmetric plates [9, 7, 8, 10, 11, 12, 13, 14, 15, 16]. Satisfied accurate predictions for the deformed shapes are achieved if the nonlinear von Kármán terms are included in mid-plane strains and sufficient number of terms in the polynomial expansion is used in the model. However, no physical insights had been given to understand why the early bending-stretching coupling can greatly enhance the large-deflection effect [5], and why some terms in the polynomials expansion of mid-plane strains are critical for obtaining the accurate solution, whereas other terms are negligible. In the study of snap-through phenomenon for cross-ply bistable composite plates, it was found that the Rayleigh-Ritz models established from the classical thin plate theory over predict the bending stiffness and the critical snap-through load [17]. The prediction for snap-through load can be improved by increasing the order of polynomials expansion in the displacement functions [13], but it often involves a large number of unknown variables. Lamacchia *et. al* [18] proposed a sophisticated numerical approach that can efficiently and accurately model the bistable plates. However, the conventional compatibility of mid-plane strains was employed in their approach, therefore the fundamental mechanism of their modeling approach remains the same compared with previous work. On the other hand, it is very difficult to establish the nonlinear dynamic model for unsymmetric plates even using the high order polynomials expansion in the displacement functions or applying a sophisticated numerical method [19]. This is because it is often very tedious to solve a set of nonlinear differential equations with many variables. The previous works are not sufficiently accurate to capture the complicated nonlinear dynamics behaviour for unsymmetric bistable plates [20, 21, 22, 23]. Establishing accurate and efficient models for analyzing the nonlinear dynamics of unsymmetric bistable plates is of critical important in the practical design of morphing structures [24, 25] and broadband vibration energy harvesting devices [26, 27]. More recently, an efficient analytical model for the nonlinear dynamics of bi-stable composite plates [19] was proposed and presented by the authors, which is partially based on the model introduced in this paper. It is also approved that this improved model for unsymmetric plates can

effectively and accurately capture the nonlinear relationship between temperature and curvature of the bistable plates with temperature dependent material properties [28, 29].

After a thorough study of many previous works on unsymmetric plates, it was found that the conflict between the unstrained mid-plane assumption in Kirchhoff-Love thin plate theory and the stretching-bending coupling of unsymmetric plates are the major reasons that lead to the inaccurate predictions for unsymmetric plates. In this study, the authors make an effort to overcome this conflict by establishing an improved model for unsymmetric plates, in which the neutral plane strains are directly utilized, or alternatively the expressions for the mid-plane strains and the corresponding compatibility equation are modified to take into account the stretching-bending coupling. In doing so, the problem of unsymmetric plates is then reduced to an analogous problem of a symmetric or isotropic plate. Subsequently, the classical Kirchhoff-Love thin plate theory is modified by following an approximating method proposed by Ashton in 1969 [30]. Instead of mid-plane strains, this study introduces the membrane strains to derive the basic geometric functions. Consequently, a new compatibility equation is derived between the out-of-plane displacement and the membrane strains. Note, as an important characteristic of the geometric functions, each component of the membrane strains of an unsymmetric plate could be in different planes. Therefore, new expressions for the mid-plane strains of an unsymmetric plate are derived from the membrane strains, and the modified compatibility equation in terms of the mid-plane strains is also derived accordingly. The paper is structured as follows. In section 2, the conflict between classical thin plate theory and the mid-plane strain based constitutive equation in modelling of unsymmetric plates is firstly illustrated. Next, an improved model that utilize the neutral plane strains as primary variables for unsymmetric plates is proposed. The new constitutive equation and modified compatibility equation based on the mid-plane strains are also derived. In section 3, the pure bending problem of unsymmetric plates for both the small deformation case and the large deformation case are studied. The corresponding modified governing equation for the small deformation problem of unsymmetric plates is derived for the general three dimensional equilibrium equations. The corresponding modified energy formula is also derived for establishing a Rayleigh-Ritz model for the large deformation problem of unsymmetric plates. The results predicted via the classical theory of plate and the modified theory of plate are compared and discussed. In section 4, the advantages of applying the new improved

model to analyze the bistable cross-ply laminates are demonstrated. With the Rayleigh-Ritz method, the stable configurations, the snap-through loads and nonlinear dynamics of the bistable cross-ply plates are predicted and validated with FEM results.

2. An improved model for unsymmetric plates

In the classical thin plate theory, the mid-plane strains are defined in terms of the in-plane displacements given by,

$$\begin{bmatrix} \varepsilon_x^0 \\ \varepsilon_y^0 \\ \gamma_{xy}^0 \end{bmatrix} = \begin{bmatrix} \frac{\partial u^0}{\partial x} \\ \frac{\partial v^0}{\partial y} \\ \frac{\partial u^0}{\partial y} + \frac{\partial v^0}{\partial x} \end{bmatrix} \quad (1)$$

where u^0 and v^0 represent the in-plane displacements of mid-planes. For a general plate, the relationship between the in-plane stress resultant \mathbf{N} , bending moment resultant \mathbf{M} and the mid-plane strains are defined by the constitutive equation as,

$$\begin{bmatrix} \mathbf{N} \\ \mathbf{M} \end{bmatrix} = \begin{bmatrix} \mathbf{A} & \mathbf{B} \\ \mathbf{B} & \mathbf{D} \end{bmatrix} \begin{bmatrix} \boldsymbol{\varepsilon}^0 \\ \mathbf{K} \end{bmatrix} \quad (2)$$

where \mathbf{A} , \mathbf{B} and \mathbf{D} represent the in-plane stretching stiffness matrix, stretching-bending stiffness matrix and bending stiffness matrix, respectively. $\mathbf{K} = [k_x, k_y, k_{xy}]^T$ represent the curvatures. For a symmetric laminate, the geometric mid-plane is also the neutral plane of the plate, and all elements of the stretching-bending stiffness matrix \mathbf{B} equal to zero. However, when the laminated plate is unsymmetric, for instance, if the laminated plies or material properties near the bottom region of the plate are much stiffer than that in the top region, the geometric mid-plane does not coincide with the neutral plane of the plate. In such a case, the neutral plane will be closer to the bottom of the plate when it is under a pure bending, as shown in Fig. 1 [31]. This also can be inferred from the constitutive equation Eq. (2), as the bending curvature gives rise to a mid-plane strain as illustrated in Fig. 1. Similarly, a mid-plane stretching strain to the unsymmetric plate result in a certain amount of bending deformation.

For unsymmetric plates, the stretching-bending stiffness matrix $\mathbf{B} \neq 0$, the in-plane strains can be written in an inverse form in terms of the in-plane

stress resultants and curvatures as,

$$\begin{bmatrix} \varepsilon_x^0 \\ \varepsilon_y^0 \\ \gamma_{xy}^0 \end{bmatrix} = \mathbf{A}^{-1}\mathbf{N} - \mathbf{A}^*\mathbf{K} = \begin{bmatrix} \varepsilon_x^m \\ \varepsilon_y^m \\ \gamma_{xy}^m \end{bmatrix} - \begin{bmatrix} A_{11}^* & A_{12}^* & A_{16}^* \\ A_{12}^* & A_{22}^* & A_{26}^* \\ A_{16}^* & A_{26}^* & A_{66}^* \end{bmatrix} \begin{bmatrix} k_x \\ k_y \\ k_{xy} \end{bmatrix} \quad (3)$$

where $\mathbf{A}^* = \mathbf{A}^{-1}\mathbf{B}$, and $\varepsilon^m = \mathbf{A}^{-1}\mathbf{N} = [\varepsilon_x^m, \varepsilon_y^m, \gamma_{xy}^m]^T$ are defined as the strains at the neutral plane, named as membrane strains in this study. For a general plate under the pure bending, the in-plane forces \mathbf{N} equal to zero. Therefore, the membrane strains ε^m defined in Eq. (3) also equals to zero. For example, if a $[0_n/90_n]$ composite plate is under a pure bending loading, Eq. (3) is reduced to,

$$\begin{bmatrix} \varepsilon_x^0 \\ \varepsilon_y^0 \\ \gamma_{xy}^0 \end{bmatrix} = \begin{bmatrix} A_{11}^*k_x + A_{12}^*k_y \\ A_{12}^*k_x - A_{11}^*k_y \\ 0 \end{bmatrix} \quad (4)$$

This nonzero mid-plane strains of this cross ply composite plate from the constitutive equation is in conflict with the assumption of classical thin plate theory, which states that the mid-plane remains unstrained after a pure bending. Substituting Eq. (4) into the compatibility equation expressed in terms of the mid-plane strains as given by,

$$\frac{\partial^2 \varepsilon_x^0}{\partial y^2} + \frac{\partial^2 \varepsilon_y^0}{\partial x^2} - \frac{\partial^2 \gamma_{xy}^0}{\partial x \partial y} \equiv 0 \quad (5)$$

In this case, the left part of Eq.(5) equals to $A_{12}^* \left(\frac{\partial^4 w}{\partial y^4} - \frac{\partial^4 w}{\partial x^4} \right)$ rather than zero. Therefore, the compatibility equation is not satisfied for the cross-ply composite plate if the geometric function for the mid-plane strains given by Eq. (1) is applied.

In the classical Kirchhoff-Love thin plate theory, an important assumption is that the in-plane displacements u and v induce identical strains to each plane of the plate along its thickness direction. In the derivation of Eq. (1) and Eq. (5), the mid-plane is also assumed to be the neutral surface. However, the conflict results derived in Eq. (4) and Eq. (5) for the $[0_n/90_n]$ composite plate indicate that it is not appropriate to use the mid-plane displacements u^0 and v^0 to represent the in-plane displacements in the model of an unsymmetric plate.

To overcome this issue, the in-plane displacements or strains at the neu-

tral plane are used as the primary model variables for the unsymmetric plates. As a consequence, the geometric function of an unsymmetric plate in a general form is represented using the following Eq. (6) instead of Eq.(1),

$$\begin{bmatrix} \varepsilon_x^m \\ \varepsilon_y^m \\ \gamma_{xy}^m \end{bmatrix} = \begin{bmatrix} \frac{\partial u}{\partial x} \\ \frac{\partial v}{\partial y} \\ \frac{\partial u}{\partial y} + \frac{\partial v}{\partial x} \end{bmatrix} \quad (6)$$

where u and v represent the in-plane displacements at the neutral surfaces, and ε_x^m , ε_y^m and γ_{xy}^m denote the membrane strains. Eq. (6) is established based on the following assumptions: plate thickness is much smaller than the other physical dimensions; normal to the neutral surfaces before deformation remain normal to the same surface after deformation; the neutral surfaces remain unstained after bending. With the use of the membrane strains ε^m , the new constitutive equation of Eq. (2) for the unsymmetric plates is then derived as the following form,

$$\begin{bmatrix} \mathbf{N} \\ \mathbf{M} \end{bmatrix} = \begin{bmatrix} \mathbf{A} & \mathbf{O} \\ \mathbf{B} & \mathbf{D}^* \end{bmatrix} \begin{bmatrix} \varepsilon^m \\ \mathbf{K} \end{bmatrix} \quad (7)$$

where $\mathbf{D}^* = \mathbf{D} - \mathbf{B}\mathbf{A}^{-1}\mathbf{B}$ is the reduced bending stiffness (RBS) matrix, and \mathbf{O} is the null matrix. Note, the improved model for unsymmetric plates given by Eq. (7) is different with the previous RBS method [30], which simply applied the reduced bending stiffness \mathbf{D}^* , ignored the stretching-bending stiffness matrix \mathbf{B} and retained the mid-plane strains ε^0 in the model.

Under this new model system, the definition for the mid-plane strains and the corresponding compatibility equations must be modified. Substituting Eq. (6) into Eq. (2), the modified geometric functions for unsymmetric plates are defined in terms of membrane strains as,

$$\begin{bmatrix} \varepsilon_x^0 \\ \varepsilon_y^0 \\ \gamma_{xy}^0 \end{bmatrix} = \begin{bmatrix} \frac{\partial u}{\partial x} \\ \frac{\partial v}{\partial y} \\ \frac{\partial u}{\partial y} + \frac{\partial v}{\partial x} \end{bmatrix} - \mathbf{A}^* \begin{bmatrix} k_x \\ k_y \\ k_{xy} \end{bmatrix} \quad (8)$$

Note, u and v represent the in-plane membrane displacements along x and y directions, respectively, and could be in different surfaces instead of a single surface. In fact, the first part of the right-hand side of Eq.(8) represents the plate as a membrane problem and the plate thickness is ignored. The second

part at right-hand side of Eq.(8) represents the stretching-bending coupling.

The following major improvements are made in the new model: firstly, additional terms of $\mathbf{A}^*\mathbf{K}$ are introduced to take into account of stretching-bending coupling, and it vanishes for symmetric plates; secondly, the membrane strains ε_x^m , ε_y^m and γ_{xy}^m could be located in the different surfaces for unsymmetric plates. Taking the cross-ply $[0_n/90_n]$ composite plate as an example, the stretching surface along the x direction is below the mid-plane, the stretching surface along the y direction is above the mid-plane, and the surface of shear strain γ_{xy}^m coincides with the mid-plane.

Eq.(8) essentially decouple the mid-plane strains of an unsymmetric plate into a stretching term and a pure bending term. In addition, the compatibility equation in terms of the mid-plane strains must also be modified by introducing the $\mathbf{A}^*\mathbf{K}$ terms. According to Eq. (8), the compatibility equation for an unsymmetric plate in terms of the mid-plane strains is modified and expressed as,

$$\frac{\partial^2 \varepsilon_x^0}{\partial y^2} + \frac{\partial^2 \varepsilon_y^0}{\partial x^2} - \frac{\partial^2 \gamma_{xy}^0}{\partial x \partial y} = \left(\begin{array}{l} (A_{11}^* + A_{22}^* - 2A_{66}^*) \frac{\partial^4 w}{\partial x^2 \partial y^2} + A_{12}^* \left(\frac{\partial^4 w}{\partial y^4} + \frac{\partial^4 w}{\partial x^4} \right) \\ + (2A_{16}^* - A_{26}^*) \frac{\partial^4 w}{\partial x \partial y^3} + (2A_{26}^* - A_{16}^*) \frac{\partial^4 w}{\partial x^3 \partial y} \end{array} \right) \quad (9)$$

Eq. (9) indicates that the compatibility equation of unsymmetric plates contains the influence of stretching-bending coupling ($\mathbf{A}^*\mathbf{K}$ terms), which is neglected in many previous studies using the classical thin plate theory, and may result in the inaccurate shape prediction of unsymmetric plates.

In the subsequent sections, different problems including the pure bending of unsymmetric plates, curing deformation of cross-ply bistable plates, static and nonlinear dynamic responses of cross-ply bistable plates are studied, using the improved theory of unsymmetric plate.

3. Pure bending of unsymmetric plates

3.1. Governing equations

In order to establish an accurate model for unsymmetric plates, the governing equations based on the improved model are derived from the general three-dimensional static equilibrium equations. The in-plane displacements u and v at the neutral planes of a thin plate under pure bending equal to

zero. Thus, the ply stresses of the thin laminate are expressed as,

$$\begin{bmatrix} \sigma_x^i \\ \sigma_y^i \\ \tau_{xy}^i \end{bmatrix} = \mathbf{Q}^i \left(\begin{bmatrix} \frac{\partial u}{\partial x} \\ \frac{\partial v}{\partial y} \\ \frac{\partial u}{\partial y} + \frac{\partial v}{\partial x} \end{bmatrix} - \mathbf{A}^* \begin{bmatrix} k_x \\ k_y \\ k_{xy} \end{bmatrix} + z \begin{bmatrix} k_x \\ k_y \\ k_{xy} \end{bmatrix} \right) \quad (10)$$

where the superscript i denotes a ply number, and Q_i is the reduced stiffness matrix of the i^{th} ply. Eq. (11) represents the static equilibrium differential equations given as,

$$\begin{aligned} \frac{\partial \sigma_x^i}{\partial x} + \frac{\partial \tau_{yx}^i}{\partial y} + \frac{\partial \tau_{zx}^i}{\partial z} &= 0 \\ \frac{\partial \sigma_y^i}{\partial y} + \frac{\partial \tau_{yx}^i}{\partial x} + \frac{\partial \tau_{zy}^i}{\partial z} &= 0 \\ \frac{\partial \sigma_z^i}{\partial z} + \frac{\partial \tau_{zx}^i}{\partial x} + \frac{\partial \tau_{zy}^i}{\partial y} &= 0 \end{aligned} \quad (11)$$

Substituting the ply stresses given in Eq. (10) into Eq. (11), the shear stresses τ_{zx}^i and τ_{zy}^i are derived by integrating along the thickness direction,

$$\begin{aligned} \tau_{zx}^i &= - \int_{-h/2}^{h/2} \left(\frac{\partial \sigma_x^i}{\partial x} + \frac{\partial \tau_{xy}^i}{\partial y} \right) dz \\ \tau_{zy}^i &= - \int_{-h/2}^{h/2} \left(\frac{\partial \sigma_y^i}{\partial y} + \frac{\partial \tau_{xy}^i}{\partial x} \right) dz \end{aligned} \quad (12)$$

The expanded expressions of τ_{zx}^i and τ_{zy}^i are presented in Eq.(A.01) in Appendix, in which $f^i(x, y)$ and $g^i(x, y)$ are derived from the boundary conditions and stress continuity at interfaces. For an unsymmetric plate with n plies, the boundary conditions for the shear stresses are given by,

$$\begin{aligned} \tau_{zx, z=-0.5h}^1 &= 0 \\ \tau_{zx, z=-0.5h+\sum_1^i t_i}^i &= \tau_{zx, z=-0.5h+\sum_1^i t_i}^{i+1} \\ \tau_{zx, z=0.5h}^n &= 0 \end{aligned} \quad (13)$$

$$\begin{aligned}
\tau_{zy,z=-0.5h}^1 &= 0 \\
\tau_{zy,z=-0.5h+\sum_1^i t_i}^i &= \tau_{zx,z=-0.5h+\sum_1^i t_i}^{i+1} \\
\tau_{zx,z=0.5h}^n &= 0 \\
(i &= 2 \sim n - 1)
\end{aligned} \tag{14}$$

where h denotes the thickness of the plate, and t_i denotes the thickness of i^{th} ply. Substituting Eqs. (13) and (14) into Eq. (11), two equations for defining the in-plane equilibrium of a general unsymmetric plate are derived and expressed in Appendix as Eq.(A.02), which is then further simplified as followings,

$$\begin{aligned}
A_{11} \frac{\partial^2 u}{\partial x^2} + 2A_{16} \frac{\partial^2 u}{\partial x \partial y} + A_{66} \frac{\partial^2 u}{\partial y^2} + A_{16} \frac{\partial^2 v}{\partial x^2} + (A_{12} + A_{66}) \frac{\partial^2 v}{\partial x \partial y} + A_{26} \frac{\partial^2 v}{\partial y^2} &= 0 \\
A_{16} \frac{\partial^2 u}{\partial x^2} + (A_{12} + A_{66}) \frac{\partial^2 u}{\partial x \partial y} + A_{26} \frac{\partial^2 u}{\partial y^2} + A_{66} \frac{\partial^2 v}{\partial x^2} + 2A_{26} \frac{\partial^2 v}{\partial x \partial y} + A_{22} \frac{\partial^2 v}{\partial y^2} &= 0
\end{aligned} \tag{15}$$

The in-plane equilibrium equations of this proposed improved plate theory for unsymmetric plates shown in Eq. (15) have the same mathematical forms with that of symmetric plates [32], if the in-plane displacements u and v are replaced by the mid-plane displacements u_0 and v_0 . However, in physics, Eq. (15) is essentially different with the equilibrium equations for symmetric plates. Eq. (15) represents the equilibrium condition for the displacement fields u and v at the neutral surfaces, which are not geometrically fixed planes as the mid-planes, and are dynamically varying with respect to the material properties, the layup and the external applied bending moment. In other words, Eq. (15) considers the stretching-bending coupling effect for the in-plane equilibrium in an implicit manner yet using an identical mathematical form of the symmetric plates.

Substituting Eq.(A.01) in Appendix into the last equation of Eq. (11), the expression for the ply transverse stress σ_z^i is derived by integration along thickness direction as,

$$\sigma_z^i = - \int \left(\frac{\partial \tau_{zx}^i}{\partial x} + \frac{\partial \tau_{zy}^i}{\partial y} \right) dz \tag{16}$$

A simplified expression of σ_z^i for the unsymmetric plates is derived and presented in Appendix, as Eq. (A.03), in which f_1, f_2, \dots, f_{13} are functions of A^*, Q_i, h, z and are constant values after the final evaluation. The unknown function $s^i(x, y)$ is then derived using the boundary conditions and stress continuity at interfaces,

$$\begin{aligned}
\sigma_{z=-0.5h}^1 &= 0 \\
\sigma_{z=-0.5h+\sum_1^i t_i}^i &= \sigma_{z=-0.5h+\sum_1^i t_i}^{n-1} \\
\sigma_{z=0.5h}^n &= -q \\
(i &= 1 \sim n-1)
\end{aligned} \tag{17}$$

where $-q$ is the pressure applied on the upside surface of the plate. The expression for the third static equation of motion for a general unsymmetric plate is then deduced by applying the stress continuity at interfaces, and takes the form of Eq.(A.04), which is further simplified as,

$$\begin{aligned}
&D_{11}^* \frac{\partial^4 w}{\partial x^4} + D_{22}^* \frac{\partial^4 w}{\partial y^4} + (D_{12}^* + D_{21}^* + 4D_{66}^*) \frac{\partial^4 w}{\partial x^2 \partial y^2} + \\
&(2D_{26}^* + 2D_{26}^*) \frac{\partial^4 w}{\partial x \partial y^3} + (2D_{16}^* + 2D_{16}^*) \frac{\partial^4 w}{\partial x^3 \partial y} - \\
&B_{11} \frac{\partial^3 u}{\partial x^3} - 3B_{16} \frac{\partial^3 u}{\partial x^2 \partial y} - (B_{12} + 2B_{66}) \frac{\partial^3 u}{\partial x \partial y^2} - (B_{26}) \frac{\partial^3 u}{\partial y^3} \\
&- B_{16} \frac{\partial^3 v}{\partial x^3} - (B_{12} + 2B_{66}) \frac{\partial^3 v}{\partial x^2 \partial y} - 3B_{26} \frac{\partial^3 v}{\partial x \partial y^2} - B_{22} \frac{\partial^3 v}{\partial y^3} = -q
\end{aligned} \tag{18}$$

Eqs. (15) and (18) constitute a full set of equilibrium equations for a general unsymmetric plate, in terms of the in-plane displacements u, v at the neutral surfaces and out-of-plane displacement w . Compared with the governing equations given by the classical thin plate theory for the unsymmetric plates [32], Eqs. (15) and (18) have much simpler forms for the governing equations of the in-plane equilibrium conditions and a similar form for the third equilibrium equation. However, in the following sections, we will demonstrate that Eqs. (15) and (18) provide a much more effective and accurate means to model the structural behaviour of unsymmetric plates than the classical thin plate theory.

3.2. Small deformation

To validate the proposed improved model for unsymmetric plates, the out-of-plane displacement w of cross-ply and angle-ply unsymmetric plates under transverse pressure are calculated. The geometry, loading and boundary conditions of the unsymmetric plates are illustrated in Fig. 2. A uniform pressure is applied on the surface of the plate, and the plate is simply supported along the four edges. The simulation results given by both the improved theory model in Eqs. (15), (18) and the classical thin plate theory in Appendix Eq. (A.06) are obtained and compared with FEA results.

The in-plane and out-of-plane displacements are expanded using the double Fourier series [32],

$$\begin{aligned}
 u &= \sum_{m=1}^{\infty} \sum_{n=1}^{\infty} S_{mn}^u \sin \frac{m\pi x}{a} \sin \frac{n\pi y}{b} \\
 v &= \sum_{m=1}^{\infty} \sum_{n=1}^{\infty} S_{mn}^v \sin \frac{m\pi x}{a} \sin \frac{n\pi y}{b} \\
 w &= \sum_{m=1}^{\infty} \sum_{n=1}^{\infty} S_{mn}^w \sin \frac{m\pi x}{a} \sin \frac{n\pi y}{b}
 \end{aligned} \tag{19}$$

The transverse loading $q(x, y)$ is also approximately expanded using the double Fourier series form as,

$$q = \sum_{m=1}^{\infty} \sum_{n=1}^{\infty} \left(\frac{4}{ab} \int_0^a \int_0^b q(x, y) \sin \frac{m\pi x}{a} \sin \frac{n\pi y}{b} dx dy \right) \sin \frac{m\pi x}{a} \sin \frac{n\pi y}{b} \tag{20}$$

Compared with the classical thin plate theory, the equilibrium equations of in-plane displacements of unsymmetric plates are decoupled from the out-of-plane displacement as shown in Eq.(15). Therefore, the in-plane displacements u and v are solved directly by substituting Eqs.(19) and (20) into Eq.(15). After solving the resulting simultaneous algebraic equations for the Fourier parameters, we find $S_{mn}^u = S_{mn}^v = 0$. Therefore, for a small deformation pure bending problem of unsymmetric plates, Eq.(18) can be further

simplified as,

$$\begin{aligned}
& D_{11}^* \frac{\partial^4 w}{\partial x^4} + D_{22}^* \frac{\partial^4 w}{\partial y^4} + (D_{12}^* + D_{21}^* + 4D_{66}^*) \frac{\partial^4 w}{\partial x^2 \partial y^2} + \\
& (2D_{26}^* + 2D_{26}^*) \frac{\partial^4 w}{\partial x \partial y^3} + (2D_{16}^* + 2D_{16}^*) \frac{\partial^4 w}{\partial x^3 \partial y} = -q
\end{aligned} \tag{21}$$

Although Eq.(21) is identical with the governing equation that is derived from the well-known Reduced Bending Stiffness (RBS) method [30], the modelling principle and physics between these two methods are essentially different. In the RBS method, the mid-plane strains are directly ignored in the definition of bending moments \mathbf{M} , while in this study Eq. (21) is strictly derived with respect to the membrane strains and no terms are ignored in the model. Only for this particular case that considers a small deformation of the bending problem, these two methods lead to the same forms of governing equations. Completely different equations will be arrived when these two methods are applied to model either a linear buckling problem or a nonlinear problem for unsymmetric plates.

In this study, the out-of-plane displacements of two cross-ply plates and two angle-ply plates, as $D_{16}^* = D_{26}^* = 0$, are predicted using both the improved theory model and the classical thin plate theory model. The cross-ply layups are $[0_{1mm}/90_{1mm}]$ and $[0_{0.5mm}/90_{0.5mm}/0_{0.5mm}/90_{0.5mm}]$. The layups for two angle-ply plates are $[60_{1mm}/-60_{1mm}]$ and $[60_{0.5mm}/-60_{0.5mm}/60_{0.5mm}/-60_{0.5mm}]$. The plates are all square plates with $0.2m \times 0.2m$. The uniform pressure applied on the plates is 10Pa. The material properties of composite plates are listed in Table. 1.

Table 1: Material properties of composite plates

| E_{11} | E_{22} | G_{12} | ν_{12} | ρ |
|----------|----------|----------|------------|-----------------------|
| 145GPa | 9.75GPa | 5.69GPa | 0.312 | 1650kg/m ³ |

For the improved theory model, substituting Eqs. (19) and (20) into Eq.(21), the unknown parameters S_{mn}^w for the out-of-plane displacements are determined. For the classical thin plate theory, the modelling results can be obtained through substituting Eqs. (19) and (20) into Eq.(A.06) and solving the three governing equations simultaneously. Note, the displacement functions are expanded to have 25 terms, i.e. in Eqs. (19) $m = 1 \sim 5$ and $n = 1 \sim 5$. The obtained results can not benefit from further increasing the terms

in the displacement functions. The predicted out-of-plane displacements for cross-ply plates and angle-ply plates are presented in Fig. (3) and Fig. (4), respectively. The predicted results are compared and validated with Finite Element Analysis (FEA) using ABAQUS. In the FEA, the plate is modeled by 1820 S4R shell elements, the deformed shape is predicted using a general ‘Static’ step with “Nlgeom” option off.

In Fig. (3) and Fig. (4), the black dots indicate FEA results, and the red and yellow continuous surfaces present the simulation results given by the classical theory model and the improved theory model, respectively. It can be seen that, for all the cases, the improved model proposed in this study yields much more accurate results than classical thin plate theory. For the cases of $[0_{1mm}/90_{1mm}]$ and $[60_{1mm}/60_{1mm}]$ with high stretching-bending coupling effects, the classical thin plate theory produces significantly inaccurate results, whereas the errors between the improved theory model and the FEA are relatively small. In previous works [4, 5], researchers had to introduce the von Kármán non-linearity even for the model of small deformation bending problems of unsymmetric plates. The improved model proposed in this study successfully avoids this issue and can be directly applied to analyze the unsymmetric plates. It is also worthy to point out, the conclusion given in the literature [33] that the RBS method is not accurate for analyzing unsymmetric plates is inaccurate, as the RBS method has the identical mathematical equations of the proposed improved model. The examples of cross-ply and angle-ply plates in this section clearly approves that the improved model based on the membrane strains is able to accurately capture the small deformation of bending problem for unsymmetric plates, while the direct application of classical thin plate theory based on the mid-plane strains is not accurate.

3.3. Large deformation

For large deformation problems, the geometric nonlinearity is taken into account and the nonlinear von Kármán terms are included into Eq. (8) as,

$$\begin{bmatrix} \varepsilon_x^0 \\ \varepsilon_y^0 \\ \gamma_{xy}^0 \end{bmatrix} = \begin{bmatrix} \frac{\partial u}{\partial x} + \frac{1}{2} \left(\frac{\partial w}{\partial x} \right)^2 \\ \frac{\partial v}{\partial y} + \frac{1}{2} \left(\frac{\partial w}{\partial y} \right)^2 \\ \frac{\partial u}{\partial y} + \frac{\partial v}{\partial x} + \frac{\partial w}{\partial x} \frac{\partial w}{\partial y} \end{bmatrix} - \mathbf{A}^* \begin{bmatrix} k_x \\ k_y \\ k_{xy} \end{bmatrix} \quad (22)$$

Eq. (22) illustrates that, the mid-plane strains of an unsymmetric plate are composed of the contributions given by membrane strains, geometric non-linearity and stretching-bending coupling effect. According to Eq. (22), the compatibility equation considering the geometric nonlinearity for an unsymmetric plate in terms of the mid-plane strains is derived and expressed as,

$$\frac{\partial^2 \varepsilon_x^0}{\partial y^2} + \frac{\partial^2 \varepsilon_y^0}{\partial x^2} - \frac{\partial^2 \gamma_{xy}^0}{\partial x \partial y} = \left(\begin{aligned} & \left(\frac{\partial^2 w}{\partial x \partial y} \right)^2 - \frac{\partial^2 w}{\partial x^2} \frac{\partial^2 w}{\partial y^2} + (A_{11}^* + A_{22}^* - 2A_{66}^*) \frac{\partial^4 w}{\partial x^2 \partial y^2} \\ & + A_{12}^* \left(\frac{\partial^4 w}{\partial y^4} + \frac{\partial^4 w}{\partial x^4} \right) + (2A_{16}^* - A_{26}^*) \frac{\partial^4 w}{\partial x \partial y^3} \\ & + (2A_{26}^* - A_{16}^*) \frac{\partial^4 w}{\partial x^3 \partial y} \end{aligned} \right) \quad (23)$$

In this study, we argue that the nonlinear geometric function and the corresponding compatibility equation for unsymmetric plates in terms of mid-plane strains need to be modified as in Eqs. (22) and (23). This argument is approved through solving few unsymmetric plates with specific layups by a similar Rayleigh-Ritz modelling procedure, which was originally introduced by Hyer [9]. For illustration purpose, a square unsymmetric plate mounted at the central is studied. The coordinate system and the boundary conditions are shown in Fig. 5, four identical forces F are applied on each corner of the plate along the vertical direction. Applying the principle of potential energy, the first variation of strain energy subtract the virtual work done is given as,

$$\delta(U - W_F) = 0 \quad (24)$$

where U denotes the internal strain energy of the plate and expressed as,

$$U = \frac{1}{2} \int_{-L_x/2}^{L_x/2} \int_{-L_x/2}^{L_x/2} \left(\begin{bmatrix} \varepsilon^0 \end{bmatrix}^T \begin{bmatrix} \mathbf{A} & \mathbf{B} \\ \mathbf{B} & \mathbf{D} \end{bmatrix} \begin{bmatrix} \varepsilon^0 \end{bmatrix} \right) dx dy \quad (25)$$

and, the virtual work of external force δW_F is expressed as,

$$\begin{aligned} \delta W_F = & F \delta w \left(\frac{L_x}{2}, \frac{L_y}{2} \right) + F \delta w \left(\frac{L_x}{2}, -\frac{L_y}{2} \right) + \\ & F \delta w \left(-\frac{L_x}{2}, \frac{L_y}{2} \right) + F \delta w \left(-\frac{L_x}{2}, -\frac{L_y}{2} \right) \end{aligned} \quad (26)$$

To verify the modified compatibility equation Eq.(23) with respect to the mid-plane strains, a $100mm \times 100mm$ square plate with the composite

layup of $[60_{1mm}/ -60_{1mm}]$ is analyzed. A truncated polynomial expansion of out-of-plane displacement is assumed as,

$$w = a_1x^2 + b_1y^2 + a_2x^4 + b_2y^4 \quad (27)$$

where a_1, a_2 and b_1, b_2 are the unknown parameters. This form of Eq. (27) makes the twist curvature k_{xy} of the plate to be zero. The particularity of the layup $[60_{1mm}/ -60_{1mm}]$ is that in the matrix \mathbf{A}^* the terms $A_{11}^* = A_{22}^* = A_{12}^* = 0$. Because of the zero twist curvature ($k_{xy} = 0$), the mid-plane strains ε_x^0 and ε_y^0 equal to the membrane strains ε_x^m and ε_y^m , which are all assumed to be zero throughout the whole plate, i.e. $\varepsilon_x^0 = \varepsilon_x^m = 0$ and $\varepsilon_y^0 = \varepsilon_y^m = 0$. Two Rayleigh-Ritz models are established for an unsymmetric plate $[60_{1mm}/ -60_{1mm}]$ based on the improved theory model and the classical thin plate theory. Note, the two models have identical terms because of the zero mid-plane normal strains. But, they have different mid-plane shear strains, which are derived based on the classical thin plate theory Eq. (27) and expressed as,

$$\gamma_{xy}^0 = (2a_1x + 4a_2x^3) (2b_1y + 4b_2y^3) \quad (28)$$

and, the other one is given by the modified compatibility equation based on the improved theory model and expressed as,

$$\gamma_{xy}^0 = (2a_1x + 4a_2x^3) (2b_1y + 4b_2y^3) - A_{16}^* (2a_1 + 12a_2x^2) - A_{26}^* (2b_1 + 12b_2y^2) \quad (29)$$

Substituting the above mid-plane shear strains of Eq. (28) and Eq. (29) and the assumed form of the out-of-plane displacement $w(x, y)$ into Eqs.(24)-(26), a group of nonlinear algebraic equations of unknown parameters are obtained. The deformation shape of $[60_{1mm}/ -60_{1mm}]$ plate can be obtained by solving the nonlinear algebraic equations. The predicted results given by the improved model and the classical theory model are compared and validated with FEA results, as shown in Fig. 4. By using the same number of unknown parameters, the improved theory model produces much more accurate predictions than the classical theory model. Fig. 6 also shows that the classical thin plate theory predicts much larger bending strength than the improved theory model. In this specific case, the only difference between the modified theory model and the classical thin plate theory model is the resultant mid-plane shear strain γ_{xy}^0 , the difference of which is due to the use

of different compatibility equations. Therefore, it approves that a direct use of the compatibility equation based on the classical thin plate theory leads to inaccurate results in model of unsymmetric plates.

To further illustrate the drawbacks of applying classical thin plate theory to model unsymmetric plates, a more general out-of-plane displacement function defined using 4th order complete polynomials is employed in the Rayleigh-Ritz model as,

$$w = a_1x^2 + b_1y^2 + a_2x^4 + b_2y^4 + e_1xy + e_2x^2y^2 + e_3xy^3 + e_4x^3y \quad (30)$$

where a_i , b_i and e_i are the unknown parameters. For a pure bending problem, the membrane strains ε_x^m and ε_y^m are zero, the mid-plane strains given by the improved theory model are derived using Eq. (22) and expressed as,

$$\begin{aligned} \varepsilon_x^0 &= -A_{11}^*k_x - A_{12}^*k_y - A_{16}^*k_{xy} \\ \varepsilon_y^0 &= -A_{21}^*k_x - A_{22}^*k_y - A_{26}^*k_{xy} \\ \gamma_{xy}^0 &= \frac{\partial \left(\int -\frac{1}{2} (w_{,x})^2 dx \right)}{\partial y} + \frac{\partial \left(\int -\frac{1}{2} (w_{,y})^2 dx \right)}{\partial x} + \frac{\partial w}{\partial x} \frac{\partial w}{\partial y} \\ &\quad - A_{16}^*k_x - A_{26}^*k_y - A_{66}^*k_{xy} \end{aligned} \quad (31)$$

Therefore, the improved model results in 8 unknown parameters in the model for the given assumption of displacement function in Eq. (30). The deformation shape of the plate under four corner forces is predicted using the Rayleigh-Ritz procedure. If the mid-plane strains ε_x^0 and ε_y^0 are used directly, appropriate forms for ε_x^0 and ε_y^0 should be assumed in the first place. Assuming that the mid-plane strains ε_x^0 and ε_y^0 have identical terms as the improved plate theory given in Eq.(31), and the mid-plane shear strain γ_{xy}^0 is derived via the classical thin plate theory and given as,

$$\begin{aligned} \varepsilon_x^0 &= c_0 + c_1x^2 + c_2y^2 + c_3xy \\ \varepsilon_y^0 &= d_0 + d_1y^2 + d_2x^2 + d_3xy \\ \gamma_{xy}^0 &= 2(c_2 + d_2)xy + \frac{1}{2}(c_3x^2 + d_3y^2) + \\ &\quad \frac{\partial \left(\int -\frac{1}{2} (w_{,x})^2 dx \right)}{\partial y} + \frac{\partial \left(\int -\frac{1}{2} (w_{,y})^2 dx \right)}{\partial x} + \frac{\partial w}{\partial x} \frac{\partial w}{\partial y} \end{aligned} \quad (32)$$

where c_i and d_i are unknown parameters. Therefore, the classical thin plate

theory leads to 16 unknown parameters in total. For considering a more general case, the plate lay-up [60_{1mm}/ - 30_{0.5mm}] with all the terms in the \mathbf{A}^* matrix are nonzero is studied. The results of the 16-parameter model Eq.(30) and Eq.(32) derived using the classical thin plate theory are compared with the 8-parameter model given by the improved theory, i.e. Eq.(30) and Eq.(31), as shown in Fig. 7. The equations are solved by the "Findroot" function in "Mathematica", and the initial values of unknown parameters are set to be zero. Although the classical theory model employs more unknown parameters that offer more degree of freedoms in capturing the deformation of unsymmetric plates, it results in much larger error than the improved model, compared with the FEA results.

If we further increase the number of unknown parameters in the classical theory model for the series expansion of mid-plane strains as,

$$\begin{aligned}
\varepsilon_x^0 &= c_0 + c_1x^2 + c_2y^2 + c_3xy + c_4x^4 + c_5y^4 + c_6x^2y^2 + c_7xy^3 + c_8x^3y \\
\varepsilon_y^0 &= d_0 + d_1y^2 + d_2x^2 + d_3xy + d_4y^4 + d_5x^4 + d_6x^2y^2 + d_7x^3y + d_8xy^3 \\
\gamma_{xy}^0 &= 2(c_2 + d_2)xy + \frac{1}{2}(c_3x^2 + d_3y^2) + 4(c_5xy^3 + d_5x^3y) \\
&\quad + \frac{2}{3}(c_6x^3y + d_6xy^3) + \frac{3}{2}(c_7x^2y^2 + d_7x^2y^2) + \frac{1}{4}(c_8x^4 + d_8y^4) \\
&\quad + \frac{\partial(\int -\frac{1}{2}(w_{,x})^2 dx)}{\partial y} + \frac{\partial(\int -\frac{1}{2}(w_{,y})^2 dx)}{\partial x} + \frac{\partial w}{\partial x} \frac{\partial w}{\partial y}
\end{aligned} \tag{33}$$

Therefore, in Eq. (33), 26 unknown parameters are used for establishing a Rayleigh-Ritz model based on the classical thin plate theory. Fig. 8 compared the prediction results given by the classical thin plate theory with 16 parameters and 26 parameters, respectively. It clearly shows that there is nearly no significant improvement by increasing the number of parameters in classical theory model.

The resultant in-plane forces N_x and N_y given by the 16-parameter classical theory model are evaluated and expressed as,

$$\begin{aligned}
N_x &= -132.45 + 497380x^2 - 1.86725 \times 10^8x^4 - 2.17853 \times 10^{10}x^6 \\
N_y &= 104.007 - 423556y^2 + 2.08198 \times 10^8y^4 - 5.05872 \times 10^{10}y^6
\end{aligned} \tag{34}$$

Eq.(34) shows that the in-plane forces along the edges of the plate are non-zero due to the constant terms. However, this conclusion is in conflict with the boundary conditions as shown in Fig. 5, as no in-plane forces have been

applied on the plate. Because the in-plane forces have a linear relationship with the in-plane strains, the simulation error induced by the classical theory model is given by the inaccurate compatibility equation rather than the inaccurate assumptions of displacements or strains. This conclusion further approves that it is unlikely to obtain an accurate prediction of deformation shape for the $[60_{1mm}/ - 30_{0.5mm}]$ unsymmetric plate through applying a classical thin theory plate. Because the improved theory model naturally decouples the stretching-bending coupling, the above issues can be successfully avoided and the zero stress boundary conditions is satisfied irrespective of the assumed forms of strains or displacements.

The 8-parameter Modified Theory Model and the 16-parameter Classical Theory Model are further employed to predict the deformation of a $100mm \times 100mm$, $[0_{1mm}/90_{0.5mm}]$ plate, and prediction results are compared with FEA in Fig. 9. Although the two theoretical models predict similar results, the Modified Theory Model predicts accurate results with less parameters.

In general, applying the improved plate theory proposed in this study for the unsymmetric plates, the pure bending problem can be solved in an analogous way that is similar with the model of symmetric plates. If no in-plane forces or in-plane boundary conditions are applied on the unsymmetric plates, it is only needed to assume an appropriate out-of-plane displacement for this improved model to predict the deformation shapes. If a classical thin plate theory is applied for the unsymmetric plates, an appropriate assumption for the mid-plane strains ε_x^0 and ε_y^0 are critical for an accurate prediction. However, it inevitably results in much more unknown parameters. When complicated boundary conditions are applied on the unsymmetric plates, it is often difficult to find the appropriate forms for the mid-plane strains ε_x^0 and ε_y^0 . Moreover, the classical compatibility equation of mid-plane strains leads to large bending strength prediction for unsymmetric plates. Although this issue can be slightly overcome by assuming higher order complete polynomials for ε_x^0 and ε_y^0 [18], nevertheless, it inevitably results in low efficiency and inaccurate results.

4. Bistable unsymmetric plates

4.1. Bistability of cross-ply plates

When a cross-ply plate cools down from the high curing temperature to the room temperature, residual thermal stress arise due to the mismatch of

the thermal expansion parameters of different plies. As a result, a cross-ply plate may have two stable configurations. The bistable cross-ply plates have been extensively studied since last decades [7, 8, 9, 13, 20, 27, 34, 35]. In this section, the bistability of cross-ply plates is studied using the improved theory model, and also compared with the classical thin plate theory. The boundary conditions and loading of the cross-ply plates are presented in Fig. 5. The structural behaviour of the plates are followed the assumption of the Kirchhoff hypothesis and plane-stress [9]. The potential energy of a composite plate is given by,

$$\begin{aligned} \Pi = & \int_{-\frac{L_x}{2}}^{\frac{L_x}{2}} \int_{-\frac{L_y}{2}}^{\frac{L_y}{2}} \int_{-\frac{t}{2}}^{\frac{t}{2}} \left[\left(\frac{1}{2} \bar{Q}_{11} \varepsilon_x^2 + \bar{Q}_{12} \varepsilon_x \varepsilon_y + \bar{Q}_{16} \varepsilon_x \gamma_{xy} + \frac{1}{2} \bar{Q}_{22} \varepsilon_y^2 + \bar{Q}_{26} \varepsilon_y \gamma_{xy} \right. \right. \\ & \left. \left. + \frac{1}{2} \bar{Q}_{66} \gamma_{xy}^2 \right) - (\bar{Q}_{11} \alpha_x + \bar{Q}_{12} \alpha_y + \bar{Q}_{16} \alpha_{xy}) \varepsilon_x \Delta T - (\bar{Q}_{12} \alpha_x + \bar{Q}_{22} \alpha_y \right. \\ & \left. + \bar{Q}_{26} \alpha_{xy}) \varepsilon_y \Delta T - (\bar{Q}_{16} \alpha_x + \bar{Q}_{26} \alpha_y + \bar{Q}_{66} \alpha_{xy}) \gamma_{xy} \Delta T \right] dx dy dz \end{aligned} \quad (35)$$

where L_x , L_y and t denote the plate length, width and thickness, respectively. \bar{Q}_{ij} are the transformed reduced stiffness values, and α_x , α_y and α_{xy} are the transformed parameters of the thermal expansion. ΔT denotes the temperature variation. Note, for a cross-ply plate, $\bar{Q}_{16} = 0$ and $\bar{Q}_{26} = 0$.

Applying the classical thin plate theory in terms of mid-plane strains, Eq. (35) is expressed as,

$$\Pi = \int_{-\frac{L_x}{2}}^{\frac{L_x}{2}} \int_{-\frac{L_y}{2}}^{\frac{L_y}{2}} \left(\frac{1}{2} \begin{bmatrix} \varepsilon^0 \\ \mathbf{K} \end{bmatrix}^T \begin{bmatrix} \mathbf{A} & \mathbf{B} \\ \mathbf{B}^T & \mathbf{D} \end{bmatrix} \begin{bmatrix} \varepsilon^0 \\ \mathbf{K} \end{bmatrix} - \begin{bmatrix} \mathbf{N}^{\Delta T} \\ \mathbf{M}^{\Delta T} \end{bmatrix}^T \begin{bmatrix} \varepsilon^0 \\ \mathbf{K} \end{bmatrix} \right) dx dy \quad (36)$$

However, if the improved theory model based on membrane strains is applied, Eq. (35) is rewritten in the following form as,

$$\Pi = \int_{-\frac{L_x}{2}}^{\frac{L_x}{2}} \int_{-\frac{L_y}{2}}^{\frac{L_y}{2}} \left(\frac{1}{2} \begin{bmatrix} \varepsilon^m \\ \mathbf{K} \end{bmatrix}^T \begin{bmatrix} \mathbf{A} & \mathbf{O} \\ \mathbf{O} & \mathbf{D} \end{bmatrix} \begin{bmatrix} \varepsilon^m \\ \mathbf{K} \end{bmatrix} - \begin{bmatrix} \mathbf{N}^{\Delta T} \\ \mathbf{M}^{\Delta T} \end{bmatrix}^T \begin{bmatrix} \frac{1}{2} \mathbf{A}^{-1} & -\mathbf{A}^* \\ \mathbf{O} & \mathbf{I} \end{bmatrix} \begin{bmatrix} \mathbf{N}^{\Delta T} \\ \mathbf{M}^{\Delta T} \end{bmatrix} \right) dx dy \quad (37)$$

where the superscript T denotes a transpose, the superscript ΔT denotes the temperature difference between the curing temperature and the room

temperature. Eq. (36) is derived from the classical theory of plate, and Eq. (37) is derived from the improved theory model. $\mathbf{N}^{\Delta\mathbf{T}}$ and $\mathbf{M}^{\Delta\mathbf{T}}$ are the resultant force and the resultant moment given by the thermal stresses. It is very interesting to note that the stretching-bending coupling matrix \mathbf{B} is eliminated naturally in this newly derived energy formula based on the improved theory model. This implies that, under this improved theory model scheme, the problem of unsymmetric plates can be solved as effectively using an analogous way of symmetric plates. A detailed derivation process of Eq. (37) is given in (A.05).

In this section, both the classical plate theory model given by Eq. (36) and the improved theory model expressed in Eq. (37) are used to analyze the bistability of unsymmetric plates. In a Rayleigh-Ritz modelling procedure, the solution stability needs to be checked via the Jacobin matrix. The equilibrium configurations are stable if and only if the Jacobin matrix is positive, as given by,

$$\left| \frac{\partial^2 \Pi}{\partial x_i^2} \right| > 0 \quad (38)$$

A sixth order out-of-plane displacement is assumed as,

$$w = a x^2 + b y^2 + a_1 x^4 + b_1 y^4 + a_2 x^6 + b_2 y^6 + e x^2 y^2 \quad (39)$$

where a_i , b_i , and e are unknown parameters. The form of w in Eq.(39) is similar with that proposed by Gigliotti *et al.* [36]. Extra term $e x^2 y^2$ is introduced to take into account the anti-classical phenomenon near the plate corners. As there exists residual thermal stress in the laminate, none zero membrane strains ε_x^m , ε_y^m are also assumed,

$$\begin{aligned} \varepsilon_x^m &= c + c_1 y^2 + c_2 y^4 + c_3 y^6 + c_4 x^2 y^2 \\ \varepsilon_y^m &= d + d_1 x^2 + d_2 x^4 + d_3 x^6 + d_4 x^2 y^2 \end{aligned} \quad (40)$$

where c_i and d_i are unknown parameters. For $[0_n/90_n]$ cross-ply plates, $A_{16}^* = A_{26}^* = A_{66}^* = 0$, $A_{11}^* = -A_{22}^*$. If applying the improved theory model in terms of mid-plane strains, the modified form of compatibility equation (23)

must be satisfied, and the mid-plane strains take the following form as,

$$\begin{aligned}
\varepsilon_x^0 &= c + c_1y^2 + c_2y^4 + c_3y^6 + c_4x^2y^2 - (A_{11}^*k_x + A_{12}^*k_y) \\
\varepsilon_y^0 &= d + d_1x^2 + d_2x^4 + d_3x^6 + d_4x^2y^2 - (A_{21}^*k_x + A_{22}^*k_y) \\
\gamma_{xy}^0 &= 4abxy + 2c_1xy + 2d_1xy + 8a_1bx^3y + \frac{2}{3}c_4x^3y + \frac{4}{3}aex^3y + 12a_2bx^5y \\
&\quad + 6d_3x^5y + \frac{24}{5}a_1ex^5y + \frac{60}{7}a_2ex^7y + 8ab_1xy^3 + 4c_2xy^3 + \frac{2}{3}d_4xy^3 \\
&\quad + \frac{4}{3}bexy^3 + 16a_1b_1x^3y^3 - \frac{4}{3}e^2x^3y^3 + 24a_2b_1x^5y^3 + 12ab_2xy^5 + 6c_3xy^5 \\
&\quad + \frac{24}{5}b_1exy^5 + 24a_1b_2x^3y^5 + 36a_2b_2x^5y^5 + \frac{60}{7}b_2exy^7
\end{aligned} \tag{41}$$

There are 17 unknown parameters that are used in the improved theory model for the bistable unsymmetric plates. Either substituting Eq.(39) and Eq.(41) into the energy formulae Eq. (36), or, substituting Eq.(39) and Eq.(40) into the new form of energy formulae Eq. (37), and applying the Rayleigh-Ritz method will lead to the same modelling solution. This method is termed as 17-parameter improved theory model.

Eq.(3) clearly indicates that the mid-plane strain ε^0 and bending curvature \mathbf{K} for an unsymmetric plate are highly coupled. If the out-of-plane displacement function w , and the mid-plane strains ε_x^0 and ε_y^0 are taken as the model variables, ε_x^0 and ε_y^0 should have terms that are determined by w due to the stretching-bending coupling. However, in all the previous studies of bistable plates [7, 8, 9, 13, 20, 27, 34, 35], the modelling of unsymmetric plates is based on the independent series expansion of ε_x^0 , ε_y^0 and w . Some researchers intended to increase the number of terms in the series expansion of mid-plane strains [13] to obtain better prediction results. However, the influence of stretching-bending coupling on the modelling variables between out-of-plane displacement w and mid-surface strains ε_x^0 and ε_y^0 have never been deliberately considered. As a result, this independent variables model is only able to produce accurate results for some very limited cases of unsymmetric plates, and often give inaccurate results for many other cases. In this section, for the illustration purpose, a similar 17-parameter model is established based on the classical thin plate theory and the conventional compatibility equation Eq. (5). Therefore, the mid-plane strains are assumed

as,

$$\begin{aligned}
\varepsilon_x^0 &= c + c_1y^2 + c_2y^4 + c_3y^6 + c_4x^2y^2 \\
\varepsilon_y^0 &= d + d_1x^2 + d_2x^4 + d_3x^6 + d_4x^2y^2 \\
\gamma_{xy}^0 &= 4abxy + 2c_1xy + 2d_1xy + 8a_1bx^3y + \frac{2}{3}c_4x^3y + \frac{4}{3}aex^3y + 12a_2bx^5y \\
&\quad + 6d_3x^5y + \frac{24}{5}a_1ex^5y + \frac{60}{7}a_2ex^7y + 8ab_1xy^3 + 4c_2xy^3 + \frac{2}{3}d_4xy^3 \\
&\quad + \frac{4}{3}bexy^3 + 16a_1b_1x^3y^3 - \frac{4}{3}e^2x^3y^3 + 24a_2b_1x^5y^3 + 12ab_2xy^5 + 6c_3xy^5 \\
&\quad + \frac{24}{5}b_1exy^5 + 24a_1b_2x^3y^5 + 36a_2b_2x^5y^5 + \frac{60}{7}b_2exy^7
\end{aligned} \tag{42}$$

The model using Eq. (39) and (42) is termed as 17-parameter classical theory model.

The Rayleigh-Ritz method is applied to solve either the 17-parameter improved theory model or 17-parameter classical theory model. For the bistable laminates, the nonlinear-coupled equations have three groups of solutions. Each group of solution represents an equilibrium configuration. In this study, the integration, differentiation, and other operations were carried out in Mathematica©. The “FindRoot” function is employed to solve the nonlinear coupled equations. Initial values of unknowns are needed for the “FindRoot” function to start the iteration, and the final equilibrium configuration then depends on the initial value of unknowns. To obtain the two stable configurations, the initial values of a and b in displacement function w are set to be $a = 5$ and $b = 0$, or $a = 0$ and $b = -5$, respectively. To obtain the unstable configuration, the initial values of a and b are set to be $a = 5$ and $b = -5$. Initial values of other parameters in assumed displacement and strain functions are all set to be zero.

4.2. Configuration and bifurcation/loss-of-bifurcation prediction

In this study, the curing temperature is 180°C, and the room temperature is 20°C. The stable configurations and profiles of a 300mm×80mm, [0_{0.5mm}/90_{0.5mm}] plate and a 150mm×150mm, [0_{0.25mm}/90_{0.25mm}] plate are predicted using both the 17-parameter improved theory model and the 17-parameter classical theory model. The obtained configurations are compared with FEM results, as illustrated in Fig. 10 and Fig. 11, respectively. Fig. 10

and Fig. 11 show that the results given by two Rayleigh-Ritz models almost coincide with each other, and match well with the FEA results.

For the stable configuration prediction, the classical theory model and the improved theory model give the similar results. The difference between the improved theory model and the classical theory model is merely the $(A_{11}^*k_x + A_{12}^*k_y)$ and $(A_{12}^*k_x + A_{22}^*k_y)$ in the mid-plane strains ε_x^0 and ε_y^0 . If k_x and k_y are constants, the two Rayleigh-Ritz models will give identical results. It is well known that the stable configuration of a cross-ply bistable plate is cylindrical [9, 16], as it is also illustrated in Fig. 10 and Fig. 11. Consequently, for a stable configuration prediction, the difference between classical theory model and improved theory model is reduced due to the principle of Rayleigh-Ritz method. Nevertheless, for the problem of bifurcation/loss-of-bifurcation prediction of cross-ply plate, superior results are obtained by the 17-parameter improved theory model, as it is illustrated in Fig. 12 and Fig. 13.

Fig. 12 presents the predicted bifurcation phenomenon of a square cross-ply $[0_{0.25mm}/90_{0.25mm}]$ plate, in which the curves represent out-of-plane displacement of the mid-point of an edge. To show a clear illustration, the deflection curves are normalized by multiplying L_x^{-1} . The bifurcation is investigated by varying the plate length L_x . Two analytical models predict similar bifurcation phenomenon for the square $[0_{0.25mm}/90_{0.25mm}]$ plate. The plate has only one stable configuration if the plate length is smaller than the critical length, and become bi-stable when the plate length is larger than the critical length. In Fig. 12, branches AB, BC and BE represent stable configurations, and branch BD represents the unstable saddle configuration. Compared with the FEA results, it illustrates that the proposed 17-parameter improved theory model predicts better results than the 17-parameter classical theory model. The difference between the two Rayleigh-Ritz models decreases with the increase of the plate length.

Fig. 13 illustrates the loss-of-bifurcation phenomenon of a rectangular $[0_{0.5mm}/90_{0.5mm}]$ plate with constant length L_x and varying width L_y . The loss-of-bifurcation is due to that the two stable configurations of a rectangular bistable plate have different values of internal strain energy [36]. For this problem, there are also three branches of deflection curves. Branches AB and CE are stable solutions, and branch CD represents unstable solutions. This rectangular cross-ply plate shows no bifurcation phenomenon as the plate width increases. Both of these two models predict the loss-of-bifurcation phenomenon, correctly. However, the 17-parameter classical theory model is

less accurate in branch AB, and the predicted critical widths for the plates to be bi-stable are not satisfied. In contrast, the improved theory model gives nearly identical results with FEA in all aspects.

4.3. Critical static snap-through load prediction

A bistable cross-ply plate snaps from one stable configuration to the other when external force is applied on it [9]. For the prediction of critical static snap-through load, the geometry and load conditions of the plate is illustrated in Fig. 5. The snap-through process is predicted by gradually increasing the corner forces F . The configurations corresponding to different values of F are predicted by the two 17-parameter Rayleigh-Ritz models. The solution stability is checked by the corresponding Jacobin matrix. The stable and unstable configurations are obtained using different initial values of unknown parameters. When the F increases up to the snap-through load, the solution given by “FindRoot” function in “Mathematica” converges to only one configuration.

The force-displacement curve of the $150mm \times 150mm$, $[0_{0.25mm}/90_{0.25mm}]$ plate is shown in Fig. 14. In this case, the solid lines represent stable configurations, and the dotted lines represent unstable configurations. Predictions show that the force-displacement curve of the $150mm \times 150mm$, $[0_{0.25mm}/90_{0.25mm}]$ plate is anti-symmetric, which illustrates that the bending strength and the snap-through events of stable configuration A and B are exactly the same. The 17-parameter classical theory model predicts high stiffness with respect to FEA. The 17-parameter classical theory model over predicts the snap-through load by 13.61%. On the other hand, the improved theory model predicts identical bending stiffness with that given by FEM, and the prediction error of snap-through load is only 4.63% compared with the FEM result.

In Fig.15, the load-displacement curves of a rectangular $150mm \times 100mm$, $[0_{0.5mm}/90_{0.5mm}]$ plate are presented. The results of 17-parameter improved theory model agree with the FEA results in all aspects. Note, the load-displacement curves in Fig. 15 are not anti-symmetric, because the two stable configurations of a rectangular bistable plate have different structural performance, e.g. bending strength and critical snap-through load. The 17-parameter classical theory models predict similar nonlinearity and snap-through characteristics as FEA, nevertheless, the predicted snap-through loads are not as accurate as those predicted by the 17-parameter improved theory model. Comparison with respect to FEM shows that the accuracy

of 17-parameter improved theory model is better than 17-parameter classical theory model, in aspect of both the bending strength and the critical snap-through load.

5. Nonlinear dynamics analysis

The advantage of the improved theory model proposed in this study is further verified on the prediction of dynamics of unsymmetric plates. Hamilton's principle is employed to establish a nonlinear dynamic model for cross-ply bi-stable composite plates. The first variation of the Lagrangian function is expressed as,

$$\int_{t_1}^{t_2} \delta (T(t) + \Pi_F(t) - \Pi(t)) dt = 0 \quad (43)$$

where $T(t)$ is the kinetic energy, $\Pi_F(t)$ is the work done by the applied force, and $\Pi(t)$ is the total potential energy, which has been given in Eq. (24). The time integration of the variation of total kinetic energy is derived as follow,

$$\int_{t_1}^{t_2} \delta T(t) dt = - \int_{t_1}^{t_2} \left(\rho \iiint \left[\frac{d^2 u(t)}{dt^2} \delta u(t) + \frac{d^2 v(t)}{dt^2} \delta v(t) + \frac{d^2 w(t)}{dt^2} \delta w(t) \right] dx dy dz \right) dt \quad (44)$$

Since the in-plane displacements $u(t)$ and $v(t)$ are very small compared with the out-of-plane displacement $w(t)$, the contribution of in-plane displacements on the kinetic energy is ignored in this study. Eq. (44) is then expressed as,

$$\int_{t_1}^{t_2} \delta T(t) dt = - \int_{t_1}^{t_2} \left(\rho h \iint \left(\frac{d^2 w(t)}{dt^2} \delta w(t) \right) dx dy \right) dt \quad (45)$$

where ρ denotes density, h is the total plate thickness. According to Hamilton's principle, the variation of Lagrangian function is expressed in the following form, which represents the nonlinear dynamics as,

$$\rho h \int_{-\frac{L_x}{2}}^{\frac{L_x}{2}} \int_{-\frac{L_y}{2}}^{\frac{L_y}{2}} \left(\frac{d^2 w(t)}{dt^2} \frac{\partial w(t)}{\partial X} \right) dy dx + \frac{\partial \Pi(t)}{\partial X} = 0 \quad (46)$$

where $X = [a(t), b(t), a_1(t), b_1(t), a_2(t), b_2(t), e(t)]^T$, Eq. (44) can be represented in a matrix form as,

$$\mathbf{M}\ddot{X} + \frac{\partial \Pi(t)}{\partial X} = 0 \quad (47)$$

where \mathbf{M} denotes the mass matrix. The expression of \mathbf{M} is presented in Appendix, as Eq.(A.07).

The nonlinear dynamics of the bistable cross-ply plate is predicted using both the 17-parameter classical theory model and the 17-parameter improved theory model, and the obtained results are compared with the FEA. Four identical concentrated forces of 1.25N are initially applied at each corner of the plate, which is mounted at the centre. The applied forces are then suddenly removed, and the dynamic characteristics of the plate are analyzed. For an illustration purposes, the $150\text{mm} \times 150\text{mm}$, $[0_{0.25\text{mm}}/90_{0.25\text{mm}}]$ bi-stable plate is studied. The static stable configurations of the bi-stable plate are predicted first, and then are used as the initial deformation for the nonlinear dynamics analysis. The dynamics response of the bi-stable plates needs to obtain the solution of Eq. (47). In this study, Eq. (47) is solved using the "NDSolve" function with an automatically selected algorithm (e.g. Runge–Kutta method) in Mathematica©. The maximum time step is set to be $1\mu\text{s}$. In the FEM analysis, damping is not considered in the analysis, the concentrated forces are first applied in the "Static" step, and are removed in the "Dynamic implicit" step. The predicted responses of both time series and FFT are presented in Fig. 16. The peak point of the frequency response near 100Hz indicates the fundamental mode of the stable configuration of plate. The 17-parameter improved Rayleigh-Ritz model leads to the similar dynamic response with that predicted by FEA. However, the 17-parameter classical theory model over predicts the first dominant frequency.

In our previous work [19], the present improved model method for unsymmetric plates is also extended to study the nonlinear dynamics of cross-ply bi-stable composite plates. The accuracy of this improved model in predicting the nonlinear dynamics of bi-stable composite plates is validated against with our experimental results. For example, the Fig. 10 in [19] shows the single well vibrations of the bi-stable plates under low level sinusoidal excitation at different frequencies. It shows that the prediction of the resonant frequency given by our improved model well matches with experimental results, albeit that this nonlinear vibration behaviour is very challenge to predict using the

classical plate theory, and very time consuming using the “dynamic implicit” in FEA.

6. Bistable unsymmetric plates with temperature dependent material properties

In this section, the improved model for unsymmetric plates is applied to study the bistability of unsymmetric plates with temperature dependent material properties [28, 29]. Hyer *et al.* [37] found that the material properties of composites are significantly varying with respect to temperature except the transverse thermal expansion (a_{22}). The variation of each material property of T300/5028 graphite–epoxy composites is curve-fitted using polynomial functions from the experimental data, as given by the Table 1 in [37]. The bifurcation phenomenon of a square ($80mm \times 80mm$) cross-ply $[0_{0.25mm}/90_{0.25mm}]$ T300/5028 composite plate with respect to continuously varying temperature conditions is studied using the proposed improved model. The obtained bifurcation curves of this square cross-ply bistable plate are illustrated in Fig. 17. Compared with the FEA results, the proposed 17-parameter improved theory model predicts more accurate bifurcation point than the 17-parameter classical theory model. Note, the accuracy given by the classical theory model will not be improved by increasing the number of terms in the shape function.

Consequently, the improved theory model is much more accurate than the classical thin plate theory in predicting the bifurcation/loss-of-bifurcation, the critical snap through loads, the temperature variation and the nonlinear dynamics for bistable unsymmetric plates, albeit both models employed 17 unknown parameters. The above results demonstrate that applying the improved theory model, modifying the constitutive equation and the compatibility equation in terms of mid-plane strains is critical for establishing an accurate model for predicting the bistable characteristics of cross-ply plates.

7. Summary

For an unsymmetric plate, the pure bending inevitably induces in-plane stretching strains due to the stretching-bending coupling. However, this is in conflict with one of the basic assumptions employed for the classical thin plate theory, i.e. the mid-plane remains unstrained during the pure bending. This study proposes an improved model for the unsymmetric plates,

in which, the in-plane strains are no longer taken at the middle planes, but on the neutral planes. In doing so, the stretching-bending coupling is decoupled and the problems for unsymmetric plates can be solved effectively and accurately. In this improved theory model, the geometric function is modified by replacing the mid-plane strains by the membrane strains and a new constitutive equation is derived.

To apply this improved model for unsymmetric plates, one can either use the newly derived forms in terms of membrane-plane strains, or alternatively, retain the use of mid-plane strains but modify the geometric function and the compatibility equation. In this study, a new set of laminate equilibrium equations in terms of displacements is derived from stress equilibrium equations. For the linear pure bending problem of unsymmetric plates, the modified equilibrium equations have the same mathematical forms with that of the well-known RBS method, but the physics are essentially different. As an alternative way of applying this improved model, the pure bending problem of unsymmetric plates with large deformation is analyzed. Numerical examples approve that the Rayleigh-Ritz models based on the improved theory model predict much more accurate results than that given by the classical thin plate theory, albeit the improved theory model uses much less number of unknown parameters. It is also shown that the classical thin plate theory based Rayleigh-Ritz models predict high bending strength for the angle-ply plates. This phenomenon indicates that the classical geometric functions induce inaccurate compatibility for the unsymmetric plates in terms of mid-plane strains.

The modified theory of plate is also verified by investigating the bistability of cross-ply plates. Two 17-parameter Rayleigh-Ritz models are respectively established based on the modified theory of plate and classical theory of plate. The two 17-parameter Rayleigh-Ritz models show equivalent accuracy on stable configuration of cross-ply bistable plate due to its nearly constant bending curvature. Nevertheless, for the further prediction on the bistable characteristics of cross-ply plates, the modified theory of plate confirms its superiority via predicting more accurate critical plate length to have bistability, snap-through load, nonlinear dynamic response and temperature variation for cross-ply bistable plates. For future research, the potential of applying proposed modified theory of plate on the buckling/post-buckling problem of unsymmetric plates will be studied.

Acknowledgments

Zhangming Wu sincerely acknowledges the financial support from A3 Talent Researcher Programme of Ningbo University, Zhejiang Province, China, and Hao Li acknowledges the support from National Natural Science Foundation of China Youth Fund, Grant No. 51605299.

A. Appendix

$$\tau_{zx}^i = \left(\begin{aligned} & f^i(x, y) - (A_{12}^* Q_{16}^i z + A_{22}^* Q_{26}^i z + A_{26}^* Q_{66}^i z - \frac{1}{2} Q_{26}^i z^2) \frac{\partial^3 w}{\partial y^3} \\ & - (A_{11}^* Q_{11}^i z + A_{12}^* Q_{12}^i z + A_{16}^* Q_{16}^i z - \frac{1}{2} Q_{11}^i z^2) \frac{\partial^3 w}{\partial x^3} \\ & - \left((A_{12}^* Q_{11}^i + A_{22}^* Q_{12}^i + A_{26}^* Q_{16}^i + 2A_{16}^* Q_{16}^i + \right. \\ & \quad \left. 2A_{26}^* Q_{26}^i + 2A_{66}^* Q_{66}^i) z - (\frac{1}{2} Q_{12}^i + Q_{66}^i) z^2 \right) \frac{\partial^3 w}{\partial x \partial y^2} \\ & - \left((A_{11}^* Q_{16}^i + A_{12}^* Q_{26}^i + A_{16}^* Q_{66}^i + 2A_{16}^* Q_{11}^i \right. \\ & \quad \left. + 2A_{26}^* Q_{12}^i + 2A_{66}^* Q_{16}^i) z - (\frac{1}{2} Q_{16}^i + Q_{16}^i) z^2 \right) \frac{\partial^3 w}{\partial x^2 \partial y} \\ & - Q_{66}^i z \frac{\partial^2 u}{\partial y^2} - Q_{26}^i z \frac{\partial^2 v}{\partial y^2} - Q_{12}^i z \frac{\partial^2 v}{\partial x \partial y} - Q_{66}^i z \frac{\partial^2 v}{\partial x \partial y} - \\ & \quad Q_{16}^i z \frac{\partial^2 u}{\partial x \partial y} - Q_{16}^i z \frac{\partial^2 u}{\partial x \partial y} - Q_{11}^i z \frac{\partial^2 u}{\partial x^2} - Q_{16}^i z \frac{\partial^2 v}{\partial x^2} \end{aligned} \right) \quad (\text{A.01a})$$

$$\tau_{zy}^i = \left(\begin{aligned} & g^i(x, y) - (A_{12}^* Q_{12}^i z + A_{22}^* Q_{22}^i z + A_{26}^* Q_{26}^i z - \frac{1}{2} Q_{22}^i z^2) \frac{\partial^3 w}{\partial y^3} \\ & - (A_{11}^* Q_{16}^i z + A_{12}^* Q_{26}^i z + A_{16}^* Q_{66}^i z - \frac{1}{2} Q_{16}^i z^2) \frac{\partial^3 w}{\partial x^3} \\ & - \left((A_{12}^* Q_{16}^i + A_{22}^* Q_{26}^i + A_{26}^* Q_{66}^i + 2A_{16}^* Q_{12}^i + \right. \\ & \quad \left. 2A_{26}^* Q_{22}^i + 2A_{66}^* Q_{26}^i) z - (\frac{1}{2} Q_{26}^i + Q_{26}^i) z^2 \right) \frac{\partial^3 w}{\partial x \partial y^2} \\ & - \left((A_{11}^* Q_{12}^i + A_{12}^* Q_{22}^i + A_{16}^* Q_{26}^i + 2A_{16}^* Q_{16}^i \right. \\ & \quad \left. + 2A_{26}^* Q_{26}^i + 2A_{66}^* Q_{66}^i) z - (\frac{1}{2} Q_{16}^i + Q_{16}^i) z^2 \right) \frac{\partial^3 w}{\partial x^2 \partial y} \\ & - Q_{26}^i z \frac{\partial^2 u}{\partial y^2} - Q_{22}^i z \frac{\partial^2 v}{\partial y^2} - Q_{26}^i z \frac{\partial^2 v}{\partial x \partial y} - Q_{26}^i z \frac{\partial^2 v}{\partial x \partial y} - \\ & \quad Q_{12}^i z \frac{\partial^2 u}{\partial x \partial y} - Q_{66}^i z \frac{\partial^2 u}{\partial x \partial y} - Q_{16}^i z \frac{\partial^2 u}{\partial x^2} - Q_{66}^i z \frac{\partial^2 v}{\partial x^2} \end{aligned} \right) \quad (\text{A.01b})$$

$$\begin{pmatrix} (-A_{12}^*A_{16} - A_{22}^*A_{26} - A_{26}^*A_{66} + B_{26}) \frac{\partial^3 w}{\partial y^3} + \\ (-A_{11}^*A_{11} - A_{12}^*A_{12} - A_{16}^*A_{16} + B_{11}) \frac{\partial^3 w}{\partial x^3} + \\ (-A_{11}^*A_{16} - A_{12}^*A_{26} - A_{16}^*A_{66} - 2A_{16}^*A_{11} - \\ 2A_{26}^*A_{12} - 2A_{66}^*A_{16} + B_{16} + 2B_{16} \frac{\partial^3 w}{\partial x^2 \partial y} + \\ (-A_{12}^*A_{11} - A_{22}^*A_{12} - A_{26}^*A_{16} - 2A_{16}^*A_{16} - \\ 2A_{26}^*A_{26} - 2A_{66}^*A_{66} + B_{12} + 2B_{66}) \frac{\partial^3 w}{\partial x \partial y^2} \\ A_{11} \frac{\partial^2 u}{\partial x^2} + 2A_{16} \frac{\partial^2 u}{\partial x \partial y} + A_{66} \frac{\partial^2 u}{\partial y^2} + A_{16} \frac{\partial^2 v}{\partial x^2} + \\ (A_{12} + A_{66}) \frac{\partial^2 v}{\partial x \partial y} + A_{26} \frac{\partial^2 v}{\partial y^2} \end{pmatrix} = 0 \quad (\text{A.02a})$$

$$\begin{pmatrix} (-A_{12}^*A_{12} - A_{22}^*A_{22} - A_{26}^*A_{26} + B_{22}) \frac{\partial^3 w}{\partial y^3} + \\ (-A_{11}^*A_{16} - A_{12}^*A_{26} - A_{16}^*A_{66} + B_{16}) \frac{\partial^3 w}{\partial y^3} \\ + (-A_{11}^*A_{12} - A_{12}^*A_{22} - A_{16}^*A_{26} - 2A_{16}^*A_{16} - \\ 2A_{26}^*A_{26} - 2A_{66}^*A_{66} + B_{12} + 2B_{66} \frac{\partial^3 w}{\partial x^2 \partial y} + \\ (-A_{12}^*A_{16} - A_{22}^*A_{26} - A_{26}^*A_{66} - 2A_{16}^*A_{12} - \\ 2A_{26}^*A_{22} - 2A_{66}^*A_{26} + B_{26} + 2B_{26} \frac{\partial^3 w}{\partial x \partial y^2} \\ A_{16} \frac{\partial^2 u}{\partial x^2} + (A_{12} + A_{66}) \frac{\partial^2 u}{\partial x \partial y} + \\ A_{26} \frac{\partial^2 u}{\partial y^2} + A_{66} \frac{\partial^2 v}{\partial x^2} + 2A_{26} \frac{\partial^2 v}{\partial x \partial y} + A_{22} \frac{\partial^2 v}{\partial y^2} \end{pmatrix} = 0 \quad (\text{A.02b})$$

$$\sigma_z^i = \begin{pmatrix} s^i(x, y) + f_1(A^*, Q^i, h, z) \frac{\partial^4 w}{\partial y^4} + f_2(A^*, Q^i, h, z) \frac{\partial^4 w}{\partial x \partial y^3} + \\ f_3(A^*, Q^i, h, z) \frac{\partial^4 w}{\partial x^2 \partial y^2} + f_4(A^*, Q^i, h, z) \frac{\partial^4 w}{\partial x^3 \partial y} + f_5(A^*, Q^i, h, z) \frac{\partial^4 w}{\partial x^4} + \\ f_6(Q^i, h) \frac{\partial^3 u}{\partial x^3} + f_7(Q^i, h) \frac{\partial^3 u}{\partial x^2 \partial y} + f_8(Q^i, h) \frac{\partial^3 u}{\partial x \partial y^2} + f_9(Q^i, h) \frac{\partial^3 u}{\partial y^3} + \\ f_{10}(Q^i, h) \frac{\partial^3 v}{\partial x^3} + f_{11}(Q^i, h) \frac{\partial^3 v}{\partial x^2 \partial y} + f_{12}(Q^i, h) \frac{\partial^3 v}{\partial x \partial y^2} + f_{13}(Q^i, h) \frac{\partial^3 v}{\partial y^3} = 0 \end{pmatrix} \quad (\text{A.03})$$

$$\left(\begin{array}{c}
- (A_{11}^* B_{11} + A_{12}^* B_{12} + A_{16}^* B_{16}) \frac{\partial^4 w}{\partial x^4} - \\
(A_{12}^* B_{12} + A_{22}^* B_{22} + A_{26}^* B_{26}) \frac{\partial^4 w}{\partial y^4} - \\
(2A_{16}^* B_{12} + 2A_{26}^* B_{22} + 2A_{66}^* B_{26} + \\
2A_{12}^* B_{16} + 2A_{22}^* B_{26} + 2A_{26}^* B_{66}) \frac{\partial^4 w}{\partial x \partial y^3} - \\
(A_{11}^* B_{12} + A_{12}^* B_{11} + A_{12}^* B_{22} + A_{22}^* B_{12} + A_{26}^* B_{16} + \\
A_{16}^* B_{26} + 4A_{16}^* B_{16} + 4A_{26}^* B_{26} + 4A_{66}^* B_{66}) \frac{\partial^4 w}{\partial x^2 \partial y^2} - \\
(2A_{16}^* B_{11} + 2A_{26}^* B_{12} + 2A_{66}^* B_{16} + \\
2A_{11}^* B_{16} + 2A_{12}^* B_{26} + 2A_{16}^* B_{66}) \frac{\partial^4 w}{\partial x^3 \partial y} + \\
D_{22} \frac{\partial^4 w}{\partial y^4} + D_{11} \frac{\partial^4 w}{\partial x^4} + (2D_{12} + 4D_{66}) \frac{\partial^4 w}{\partial x^2 \partial y^2} + \\
4D_{26} \frac{\partial^4 w}{\partial x \partial y^3} + 4D_{16} \frac{\partial^4 w}{\partial x^3 \partial y} - \\
B_{11} \frac{\partial^3 u}{\partial x^3} - 3B_{16} \frac{\partial^3 u}{\partial x^2 \partial y} - (B_{12} + 2B_{66}) \frac{\partial^3 u}{\partial x \partial y^2} - B_{26} \frac{\partial^3 u}{\partial y^3} - \\
B_{16} \frac{\partial^3 v}{\partial x^3} - (B_{12} + 2B_{66}) \frac{\partial^3 v}{\partial x^2 \partial y} - 3B_{26} \frac{\partial^3 v}{\partial x \partial y^2} - B_{22} \frac{\partial^3 v}{\partial y^3}
\end{array} \right) = -q \quad (\text{A.04})$$

$$\begin{aligned}
\Pi &= \iint \left(\frac{1}{2} \begin{bmatrix} \varepsilon^0 \\ \mathbf{K} \end{bmatrix}^T \begin{bmatrix} \mathbf{A} & \mathbf{B} \\ \mathbf{B} & \mathbf{D} \end{bmatrix} \begin{bmatrix} \varepsilon^0 \\ \mathbf{K} \end{bmatrix} \right) dx dy \\
&= \iint \left(\frac{1}{2} \begin{bmatrix} (\varepsilon^m - \mathbf{A}^{-1} \mathbf{B} \mathbf{K})^T & \mathbf{K}^T \end{bmatrix} \begin{bmatrix} \mathbf{A} & \mathbf{B} \\ \mathbf{B} & \mathbf{D} \end{bmatrix} \begin{bmatrix} (\varepsilon^m - \mathbf{A}^{-1} \mathbf{B} \mathbf{K}) \\ \mathbf{K} \end{bmatrix} \right) dx dy \\
&= \iint \left(\frac{1}{2} \begin{bmatrix} (\varepsilon^m - \mathbf{A}^{-1} \mathbf{B} \mathbf{K})^T \mathbf{A} + \mathbf{K}^T \mathbf{B} & (\varepsilon^m - \mathbf{A}^{-1} \mathbf{B} \mathbf{K})^T \mathbf{B} + \mathbf{K}^T \mathbf{D} \\ (\varepsilon^m - \mathbf{A}^{-1} \mathbf{B} \mathbf{K}) \\ \mathbf{K} \end{bmatrix} \right) dx dy \quad (\text{A.05}) \\
&= \iint \left(\frac{1}{2} \begin{bmatrix} (\varepsilon^m)^T \mathbf{A} & (\varepsilon^m)^T \mathbf{B} + (\mathbf{K})^T \mathbf{D}^* \end{bmatrix} \begin{bmatrix} (\varepsilon^m - \mathbf{A}^{-1} \mathbf{B} \mathbf{K}) \\ \mathbf{K} \end{bmatrix} \right) dx dy \\
&= \iint \left(\frac{1}{2} \begin{bmatrix} (\varepsilon^m)^T \mathbf{A} \varepsilon^m + (\mathbf{K})^T \mathbf{D}^* \mathbf{K} \end{bmatrix} \right) dx dy \\
&= \iint \left(\frac{1}{2} \begin{bmatrix} (\varepsilon^m)^T & \mathbf{K}^T \end{bmatrix} \begin{bmatrix} \mathbf{A} & \mathbf{O} \\ \mathbf{O} & \mathbf{D} \end{bmatrix} \begin{bmatrix} (\varepsilon^m) \\ \mathbf{K} \end{bmatrix} \right) dx dy
\end{aligned}$$

$$\begin{aligned}
& A_{11} \frac{\partial^2 u^0}{\partial x^2} + 2A_{16} \frac{\partial^2 u^0}{\partial x \partial y} + A_{66} \frac{\partial^2 u^0}{\partial y^2} + A_{16} \frac{\partial^2 v^0}{\partial x^2} + (A_{12} + A_{66}) \frac{\partial^2 v^0}{\partial x \partial y} + A_{26} \frac{\partial^2 v^0}{\partial y^2} \\
& \quad - B_{11} \frac{\partial^3 w}{\partial x^3} - 3B_{16} \frac{\partial^3 w}{\partial x^2 \partial y} - (B_{12} + 2B_{66}) \frac{\partial^3 w}{\partial x \partial y^2} - B_{26} \frac{\partial^3 w}{\partial y^3} = 0 \\
& A_{16} \frac{\partial^2 u^0}{\partial x^2} + (A_{12} + A_{66}) \frac{\partial^2 u^0}{\partial x \partial y} + A_{26} \frac{\partial^2 u^0}{\partial y^2} + A_{66} \frac{\partial^2 v^0}{\partial x^2} + 2A_{26} \frac{\partial^2 v^0}{\partial x \partial y} + A_{22} \frac{\partial^2 v^0}{\partial y^2} \\
& \quad - B_{16} \frac{\partial^3 w}{\partial x^3} - 3B_{26} \frac{\partial^3 w}{\partial x \partial y^2} - (B_{12} + 2B_{66}) \frac{\partial^3 w}{\partial x^2 \partial y} - B_{22} \frac{\partial^3 w}{\partial y^3} = 0 \quad (\text{A.06}) \\
& D_{22} \frac{\partial^4 w}{\partial y^4} + D_{11} \frac{\partial^4 w}{\partial x^4} + (2D_{12} + 4D_{66}) \frac{\partial^4 w}{\partial x^2 \partial y^2} + 4D_{26} \frac{\partial^4 w}{\partial x \partial y^3} + 4D_{16} \frac{\partial^4 w}{\partial x^3 \partial y} \\
& \quad - B_{11} \frac{\partial^3 u^0}{\partial x^3} - 3B_{16} \frac{\partial^3 u^0}{\partial x^2 \partial y} - (B_{12} + 2B_{66}) \frac{\partial^3 u^0}{\partial x \partial y^2} - B_{26} \frac{\partial^3 u^0}{\partial y^3} \\
& \quad - B_{16} \frac{\partial^3 v^0}{\partial x^3} - (B_{12} + 2B_{66}) \frac{\partial^3 v^0}{\partial x^2 \partial y} - 3B_{26} \frac{\partial^3 v^0}{\partial x \partial y^2} - B_{22} \frac{\partial^3 v^0}{\partial y^3} = q
\end{aligned}$$

$$M_{ij} = \rho h \int_{-\frac{L_x}{2}}^{\frac{L_x}{2}} \int_{-\frac{L_y}{2}}^{\frac{L_y}{2}} \left(\frac{\partial w(t)}{\partial X_j} \frac{\partial w(t)}{\partial X_i} \right) dx dy; \quad i, j = 1 \sim 7 \quad (\text{A.07})$$

where ρ denotes plate density, L_x and L_y are the plate dimensions, n is the number of unknown parameter.

References

- [1] S. P. Timoshenko, S. Woinowsky-Krieger, Theory of Plates and Shells, Mc Graw Hill India, 1969.
- [2] R. Chennamsetti, Theory of plates, presentation.
- [3] L. P. Kollár, G. S. Springer, Mechanics of Composite Structures, Cambridge University Press, 2010.
- [4] C. T. SUN, H. CHIN, Analysis of asymmetric composite laminates, AIAA Journal 26 (6) (1988) 714–718.
- [5] C. Sun, H. Chin, On large deflection effects in unsymmetric cross-ply composite laminates, Journal of Composite Materials 22 (11) (1988) 1045–1059. doi:10.1177/002199838802201103.
- [6] H.-P. Chen, J. Shu, Cylindrical bending of unsymmetric composite laminates, AIAA journal 30 (5) (1992) 1438 – 1440.

- [7] L. J. B. Peeters, P. C. Powell, L. Warnet, Thermally-induced shapes of unsymmetric laminates, *Journal of Composite Materials* 30 (5) (1996) 603–626. doi:10.1177/002199839603000504.
- [8] M.-L. Dano, M. W. Hyer, Thermally-induced deformation behavior of unsymmetric laminates, *International Journal of Solids and Structures* 35 (17) (1998) 2101 – 2120. doi:https://doi.org/10.1016/S0020-7683(97)00167-4.
- [9] M. W. Hyer, Calculations of the room-temperature shapes of unsymmetric laminates, *Journal of Composite Materials* 15 (4) (1981) 296–310. doi:10.1177/002199838101500401.
- [10] M. Schlecht, K. Schulte, Advanced calculation of the room-temperature shapes of unsymmetric laminates, *Journal of Composite Materials* 33 (16) (1999) 1472–1490. doi:10.1177/002199839903301601.
- [11] S. Aimmanee, M. W Hyer, Analysis of the manufactured shape of rectangular thunder-type actuators, *Smart Materials and Structures* 13 (2004) 1389. doi:10.1088/0964-1726/13/6/010.
- [12] F. Mattioni, P. Weaver, M. Friswell, K. Potter, Modelling and applications of thermally induced multistable composites with piecewise variation of lay-up in the planform, Vol. 7, 2007. doi:10.2514/6.2007-2262.
- [13] A. Pirrera, D. Avitabile, P. Weaver, Bistable plates for morphing structures: A refined analytical approach with high-order polynomials, *International Journal of Solids and Structures* 47 (25) (2010) 3412 – 3425. doi:https://doi.org/10.1016/j.ijsolstr.2010.08.019.
- [14] E. Eckstein, A. Pirrera, P. Weaver, Morphing high-temperature composite plates utilizing thermal gradients, *Composite Structures* 100 (2013) 363 – 372. doi:https://doi.org/10.1016/j.compstruct.2012.12.049.
- [15] M. Cantera, J. Romera, I. Adarraga, F. Mujika, Modelling of [0/90] laminates subject to thermal effects considering mechanical curvature and through-the-thickness strain, *Composite Structures* 110 (2014) 77 – 87. doi:https://doi.org/10.1016/j.compstruct.2013.11.023.

- [16] M. W. Hyer, The room-temperature shapes of four-layer unsymmetric cross-ply laminates, *Journal of Composite Materials* 16 (4) (1982) 318–340. doi:10.1177/002199838201600406.
- [17] C. G. Diaconu, P. Weaver, A. Arrieta, Dynamic analysis of bi-stable composite plates, *Journal of Sound and Vibration* 322 (2009) 987–1004. doi:10.1016/j.jsv.2008.11.032.
- [18] E. Lamacchia, A. Pirrera, I. Chenchiah, P. Weaver, Morphing shell structures: A generalised modelling approach, *Composite Structures* 131 (2015) 1017 – 1027. doi:https://doi.org/10.1016/j.compstruct.2015.06.051.
- [19] Z. Wu, H. Li, M. I. Friswell, Advanced nonlinear dynamic modelling of bi-stable composite plates, *Composite Structures* 201 (2018) 582 – 596. doi:https://doi.org/10.1016/j.compstruct.2018.06.072.
- [20] A. Arrieta, S. Neild, D. Wagg, Nonlinear dynamic response and modeling of a bi-stable composite plate for applications to adaptive structures, *Nonlinear Dynamics* 58 (2009) 259–272. doi:10.1007/s11071-009-9476-1.
- [21] A. F. Arrieta, S. A. Neild, D. J. Wagg, On the cross-well dynamics of a bi-stable composite plate, *Journal of Sound and Vibration* 330 (14) (2011) 3424 – 3441. doi:https://doi.org/10.1016/j.jsv.2011.02.006.
- [22] A. Arrieta, G. Spelsberg-Korspeter, P. Hagedorn, S. Neild, D. Wagg, Low order model for the dynamics of bi-stable composite plates, *Journal of Intelligent Material Systems and Structures* 22 (2011) 2025 – 2043. doi:10.1177/1045389X11422104.
- [23] D. N. Betts, R. Guyer, P.-Y. Le Bas, C. Bowen, D. Inman, H. A. Kim, Modelling the dynamic response of bistable composite plates for piezo-electric energy harvesting, 2014. doi:10.2514/6.2014-0154.
- [24] C. G. Diaconu, P. M. Weaver, F. Mattioni, Concepts for morphing airfoil sections using bi-stable laminated composite structures, *Thin-Walled Structures* 46 (6) (2008) 689 – 701. doi:https://doi.org/10.1016/j.tws.2007.11.002.

- [25] M.-L. Dano, M. Jean-St-Laurent, A. Fecteau, Morphing of bistable composite laminates using distributed piezoelectric actuators, *Smart Materials Research* 2012 (05 2012). doi:10.1155/2012/695475.
- [26] H. Li, F. Dai, S. Du, Broadband energy harvesting by exploiting nonlinear oscillations around the second vibration mode of a rectangular piezoelectric bistable laminate, *Smart Materials and Structures* 24 (4) (2015) 045024. doi:10.1088/0964-1726/24/4/045024.
- [27] S. Emam, D. Inman, A review on bistable composite laminates for morphing and energy harvesting, *Applied Mechanics Reviews* 67 (11 2015). doi:10.1115/1.4032037.
- [28] C. J. Brampton, D. N. Betts, C. R. Bowen, H. A. Kim, Sensitivity of bistable laminates to uncertainties in material properties, geometry and environmental conditions, *Composite Structures* 102 (2013) 276 – 286. doi:https://doi.org/10.1016/j.compstruct.2013.03.005.
- [29] P. F. Giddings, C. R. Bowen, A. I. Salo, H. A. Kim, A. Ive, Bistable composite laminates: Effects of laminate composition on cured shape and response to thermal load, *Composite Structures* 92 (9) (2010) 2220 – 2225, fifteenth International Conference on Composite Structures. doi:https://doi.org/10.1016/j.compstruct.2009.08.043.
- [30] J. Ashton, Approximate solutions for unsymmetrically laminated plates, *Journal of Composite Materials* 3 (1) (1969) 189–191. doi:10.1177/002199836900300117.
- [31] A. T. Nettles, Basic mechanics of laminated composite plates, NASA Reference Publication NASA-RP-1351, M-764, NAS 1.61:1351 (October 01, 1994).
- [32] J. M. Whitney, *Structural Analysis of Laminated Anisotropic Plates*, CRC Press, 1987.
- [33] M. Ewing, R. Hinger, A. Leissa, On the validity of the reduced bending stiffness method for laminated composite plate analysis, *Composite Structures* 9 (4) (1988) 301 – 317.

- [34] M. Schlecht, K. Schulte, M. Hyer, Advanced calculation of the room-temperature shapes of thin unsymmetric composite laminates, *Composite Structures* 32 (1) (1995) 627 – 633, eighth International Conference on Composite Structures. doi:[https://doi.org/10.1016/0263-8223\(95\)00080-1](https://doi.org/10.1016/0263-8223(95)00080-1).
- [35] L. Ren, A. Parvizi-Majidi, Z. Li, Cured shape of cross-ply composite thin shells, *Journal of Composite Materials* 37 (20) (2003) 1801–1820. doi:[10.1177/002199803035184](https://doi.org/10.1177/002199803035184).
- [36] M. Gigliotti, M. R. Wisnom, K. D. Potter, Loss of bifurcation and multiple shapes of thin [0/90] unsymmetric composite plates subject to thermal stress, *Composites Science and Technology* 64 (1) (2004) 109 – 128. doi:[https://doi.org/10.1016/S0266-3538\(03\)00213-6](https://doi.org/10.1016/S0266-3538(03)00213-6).
- [37] M. Hyer, C. Herakovich, S. Milkovich, J. Short, Temperature dependence of mechanical and thermal expansion properties of t300/5208 graphite/epoxy, *Composites* 14 (3) (1983) 276 – 280. doi:[https://doi.org/10.1016/0010-4361\(83\)90016-2](https://doi.org/10.1016/0010-4361(83)90016-2).

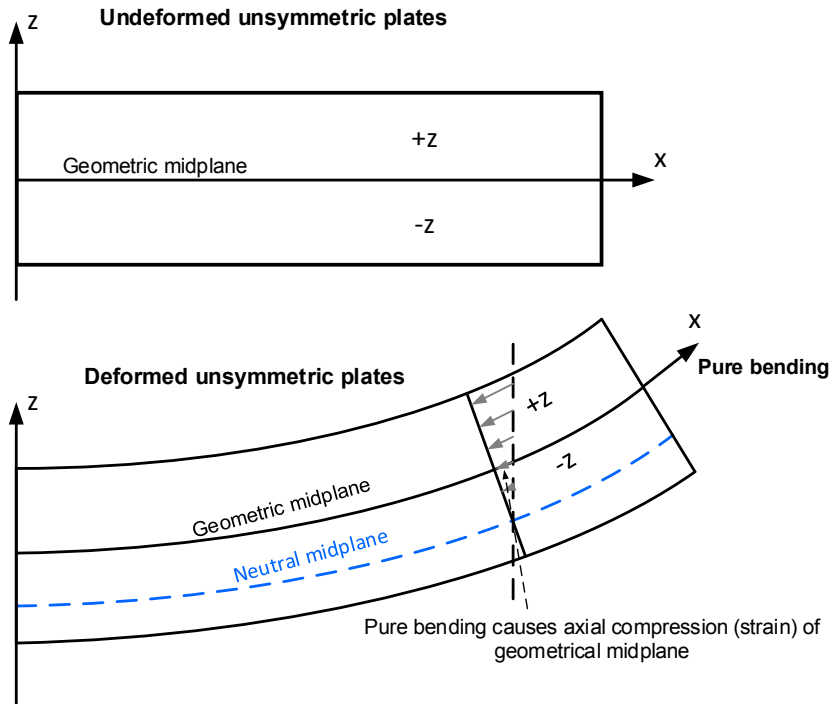


Figure 1: Transverse deformation in an unsymmetric plate, and an illustration of its mid-plane and neutral plane.

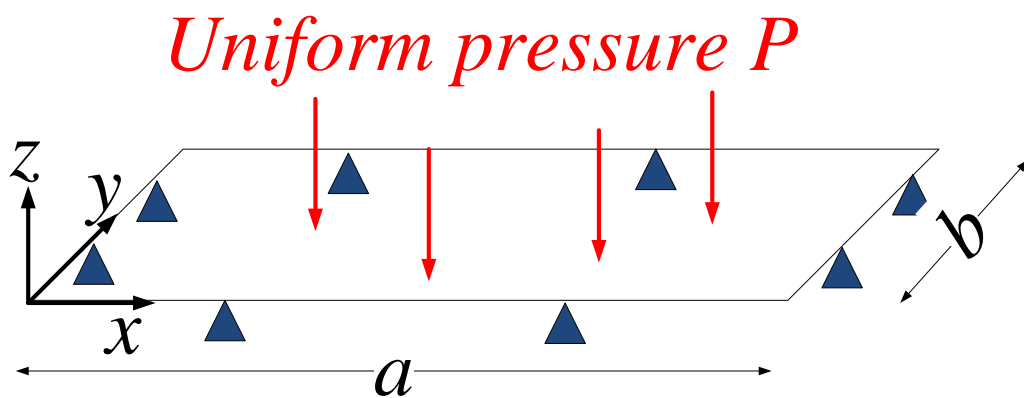


Figure 2: An illustration of a plate simply supported at edges

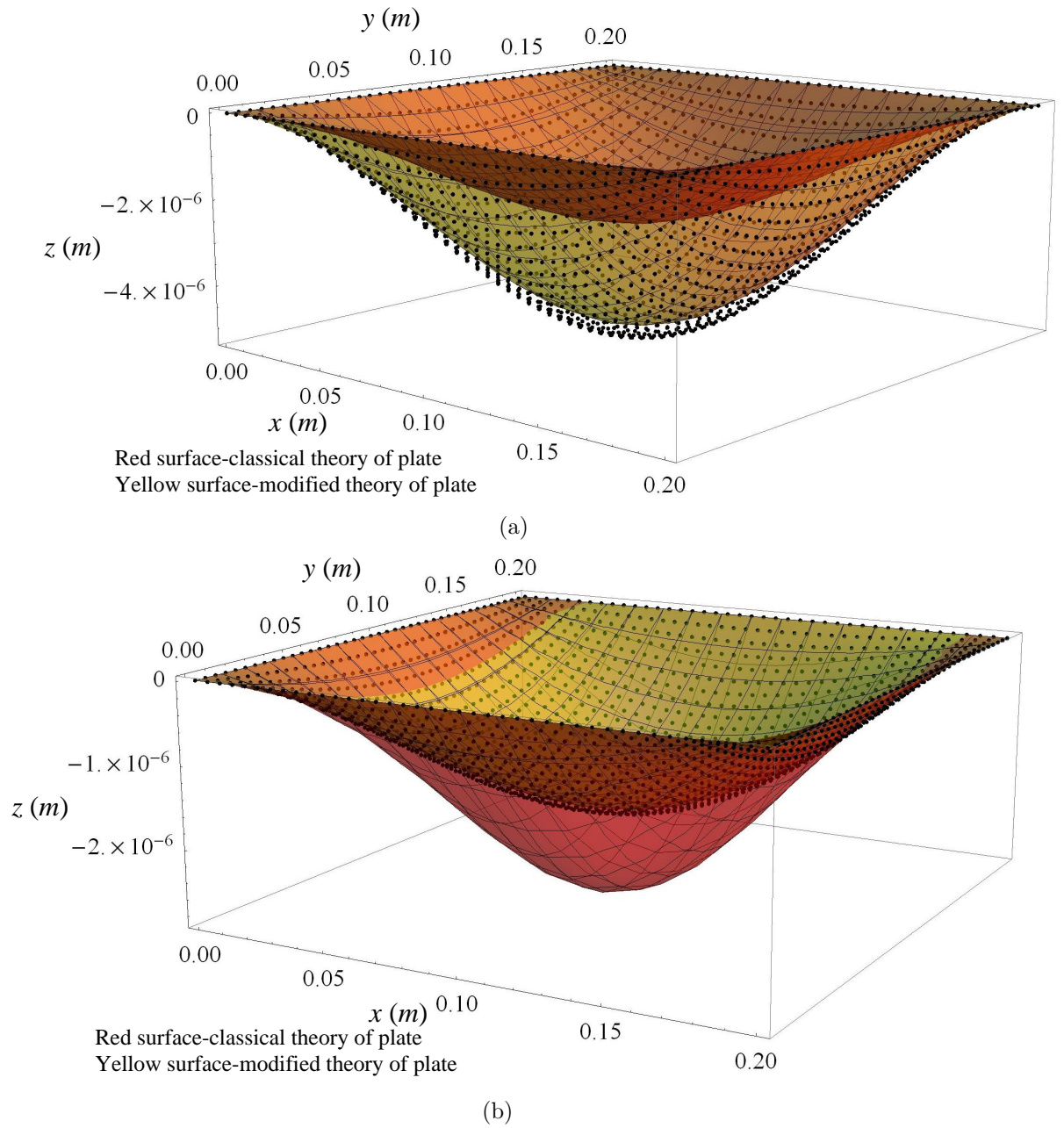
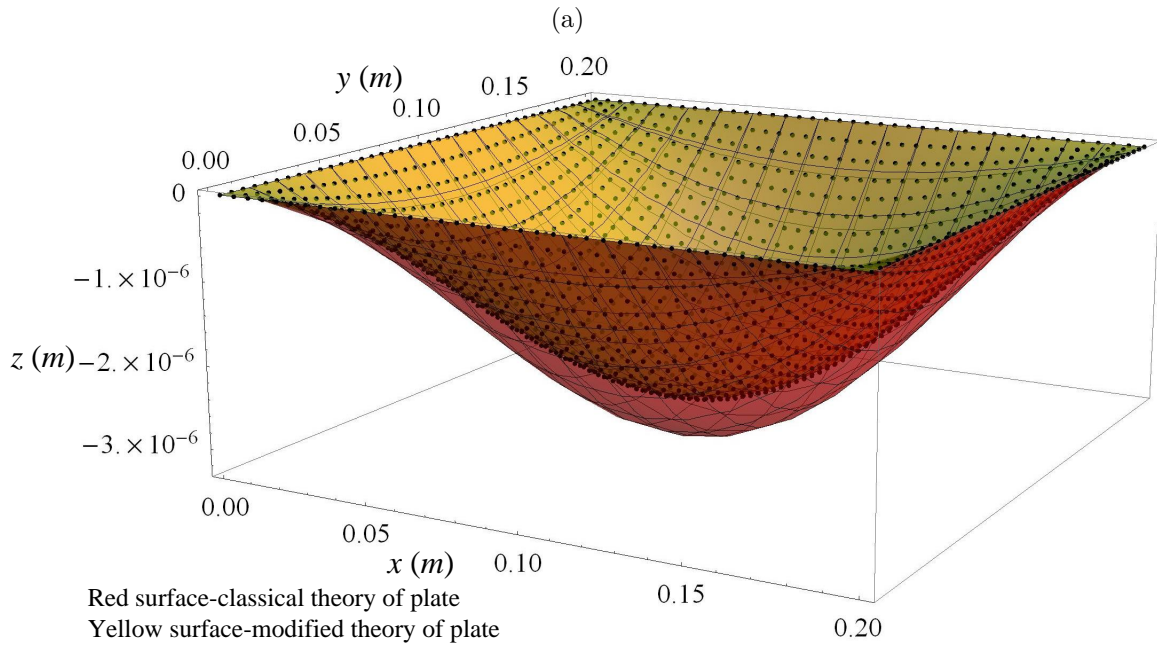
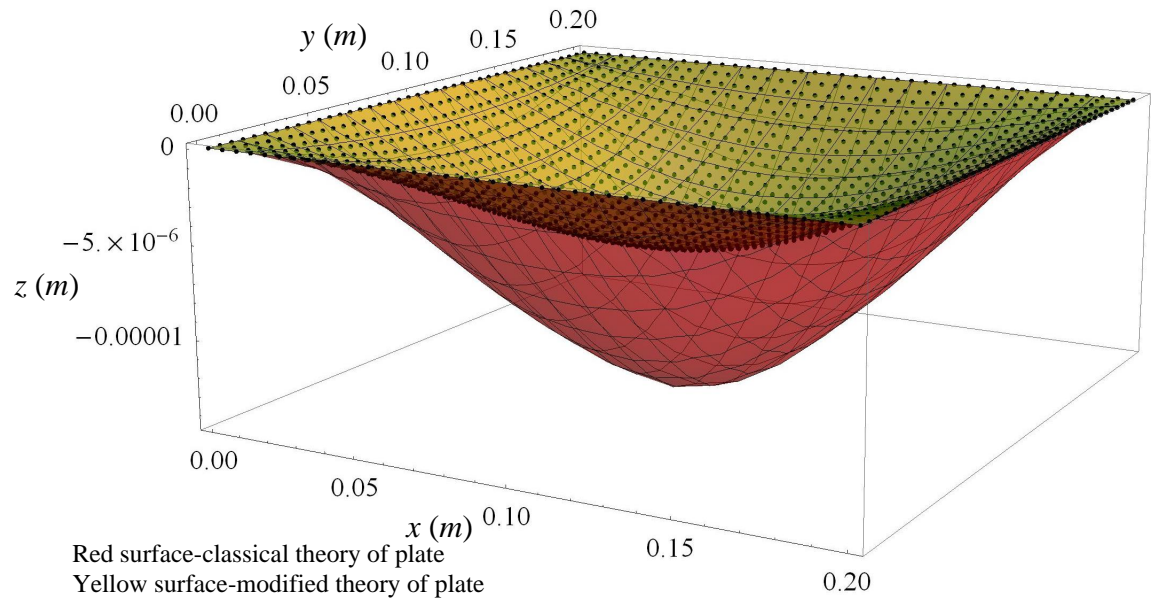


Figure 3: Predicted out-of-plane displacement of $0.2m \times 0.2m$ cross-ply plates with the uniform surface pressure of 10Pa . The black dots represent FEA results, and the continuous surface is predicted by the static equation of motion. (a): $[0_{1mm}/90_{1mm}]$ plate (b): $[0_{0.5mm}/90_{0.5mm}/0_{0.5mm}/90_{0.5mm}]$ plate.



(b)

Figure 4: Predicted out-of-plane displacement of $0.2m \times 0.2m$ angle-ply plates with the uniform surface pressure of 10Pa . The black dots represent FEA results, and the continuous surface is predicted by the surface differential equations. (a): $[60_{1mm} / -60_{1mm}]$ plate (b): $[60_{0.5mm} / -60_{0.5mm} / 60_{0.5mm} / -60_{0.5mm}]$ plate.

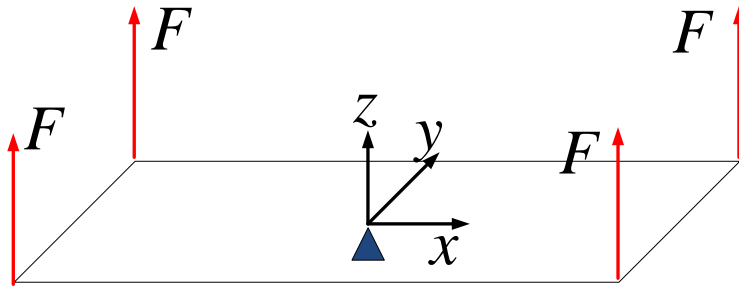


Figure 5: The sketch map of a square unsymmetric plate mounted at its central.

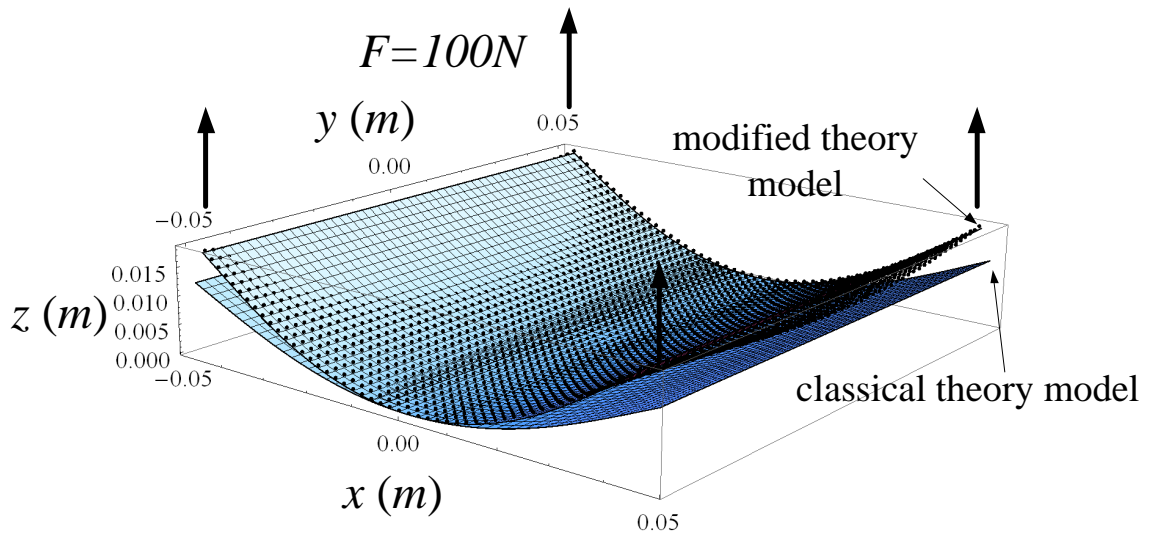


Figure 6: Predicted shape of $100\text{mm} \times 100\text{mm}$, $[60_{1\text{mm}}/-60_{1\text{mm}}]$ plate under concentrating forces. The black dots represent FEA results, and the continuous surface is predicted by the Improved Theory Model and Classical Theory Model, respectively.

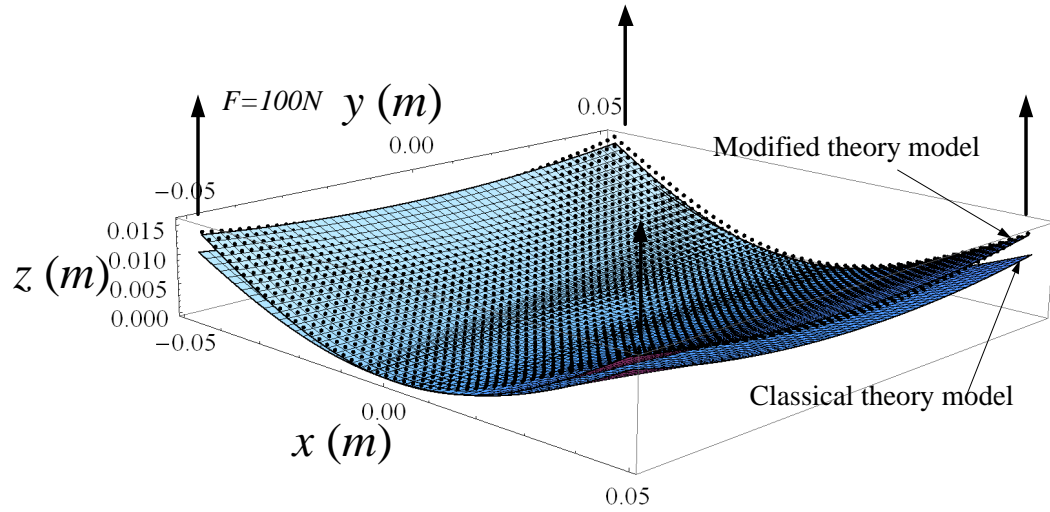


Figure 7: Predicted shape of $100\text{mm} \times 100\text{mm}$, $[60_{1\text{mm}} / -30_{0.5\text{mm}}]$ plate under concentrating forces. The black dots represent FEA results, and the continuous surfaces are predicted by Improved Theory Model and Classical Theory Model, respectively.

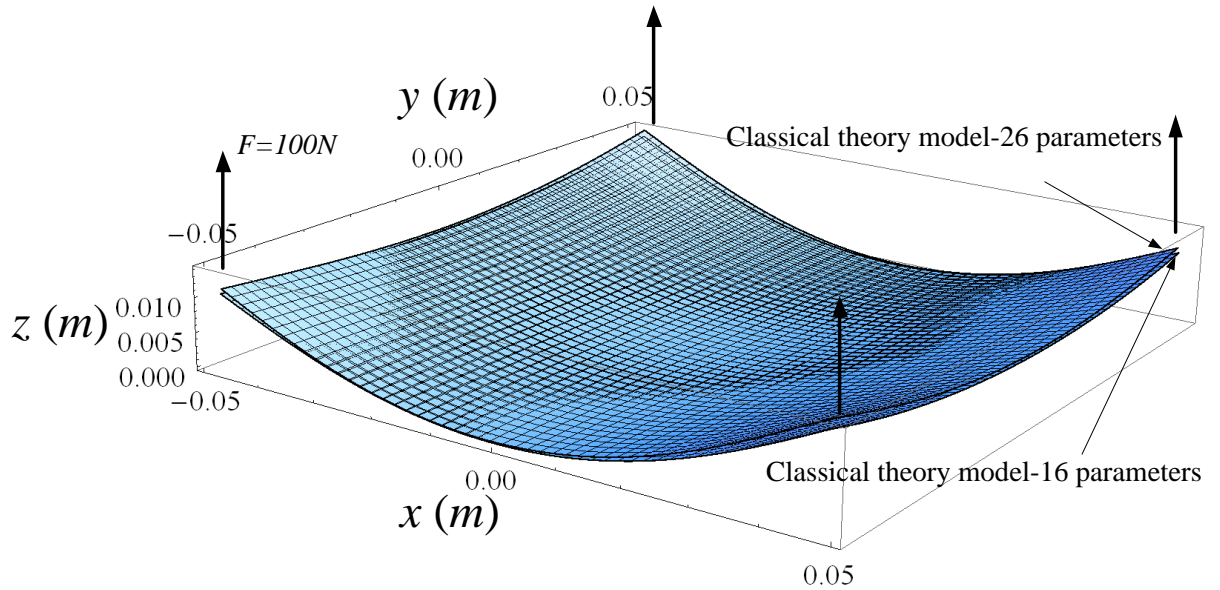


Figure 8: Comparing of the 16-parameter Classical Theory Model and the 26-parameter Classical Theory Model for $100\text{mm} \times 100\text{mm}$, $[60_{1\text{mm}} / -30_{0.5\text{mm}}]$ plate.

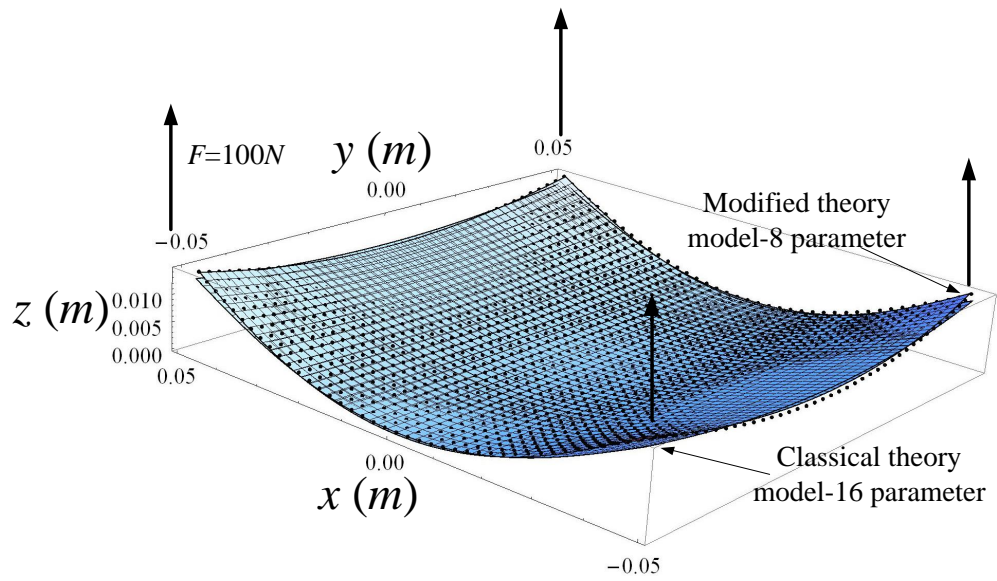


Figure 9: Predicted shapes of $100\text{mm} \times 100\text{mm}$, $[0_{1\text{mm}}/90_{0.5\text{mm}}]$ plate under concentrating forces. The black dots represent FEA results, and the continuous surfaces are predicted by the Improved Theory Model and the Classical Theory Model, respectively.

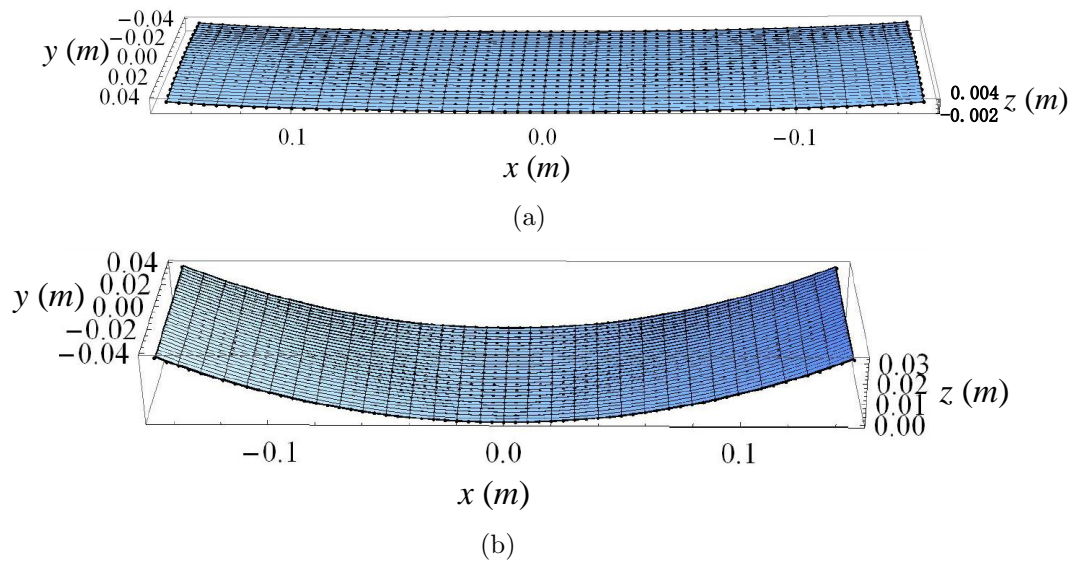


Figure 10: Stable configurations of $300\text{mm} \times 80\text{mm}$, $[0_{0.5\text{mm}}/90_{0.5\text{mm}}]$ plate. The black dots represent FEA results, and the continuous surfaces are predicted by 17-parameter improved theory model and 17-parameter classical theory model. The results of two theoretical models overlap in the figure.

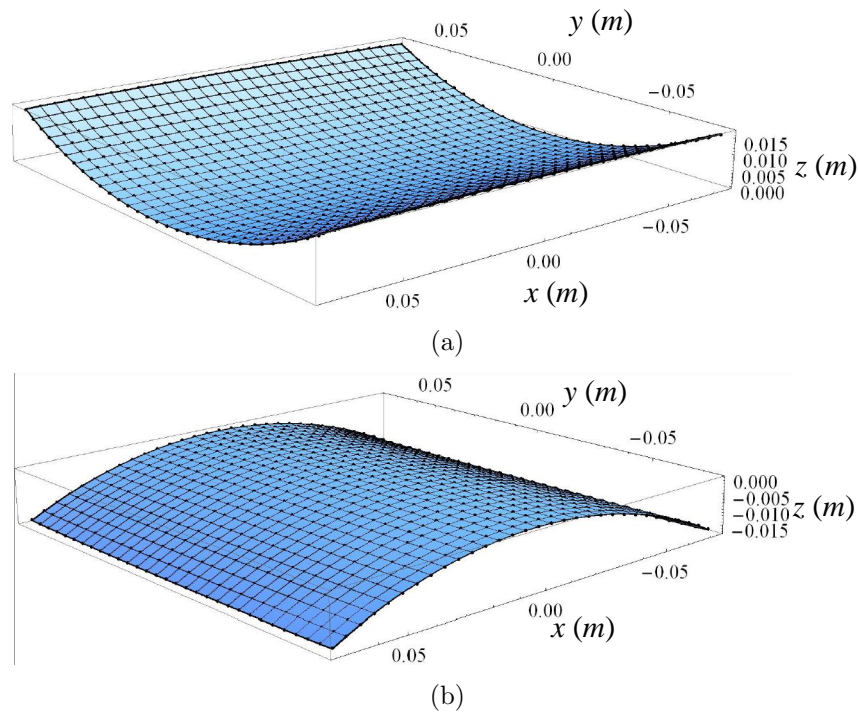


Figure 11: Stable configurations of $150\text{mm} \times 150\text{mm}$, $[0_{0.25\text{mm}}/90_{0.25\text{mm}}]$ plate. The black dots represent FEA results, and the continuous surfaces are predicted by 17-parameter modified theory model and 17-parameter classical theory model. The results of two theoretical models overlap in the figure.

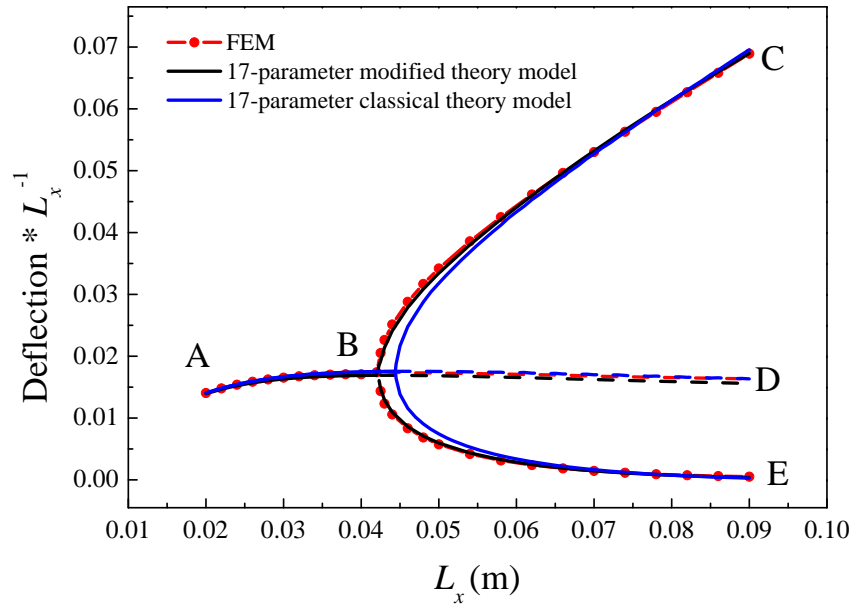


Figure 12: Normalized out-of-plane deflections of middle points at the edges of $[0_{0.5mm}/90_{0.5mm}]_T$ plates.

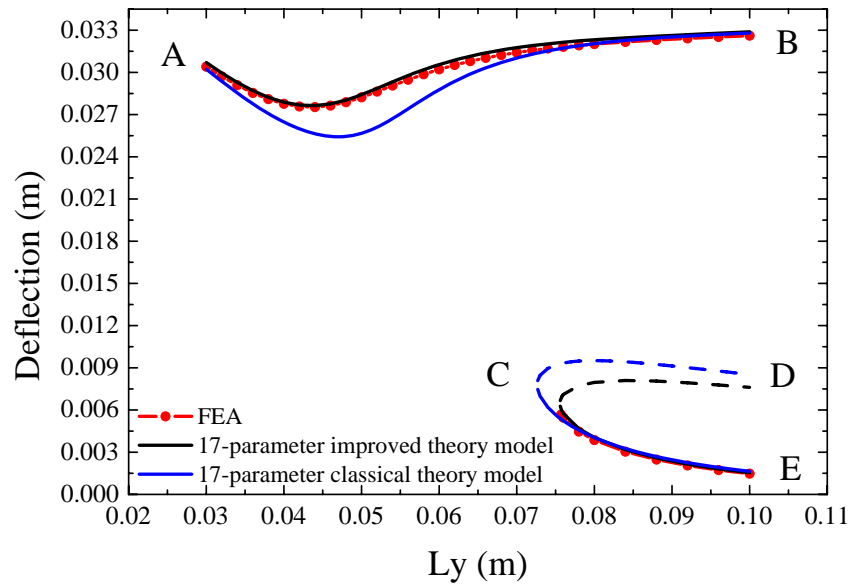


Figure 13: Out-of-plane deflections of middle points at the transverse edges of $[0_{0.5mm}/90_{0.5mm}]$ plates with constant length ($L_x = 300mm$).

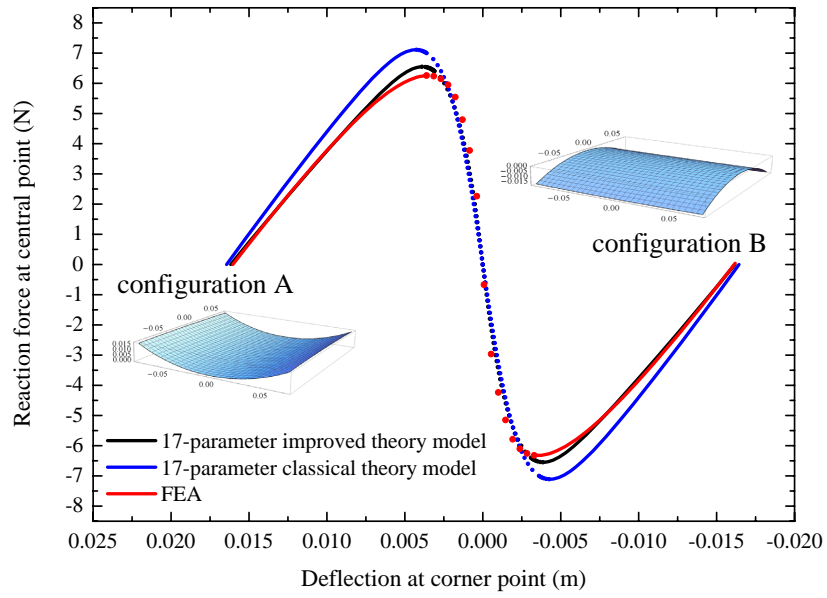


Figure 14: Load-displacement curve of $150\text{mm} \times 100\text{mm}$, $[0_2/90_2]_T$ plate mounted at central.

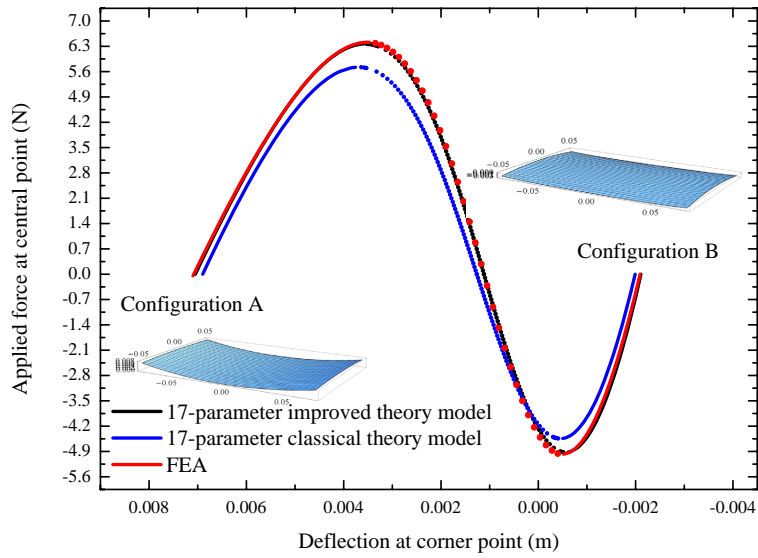
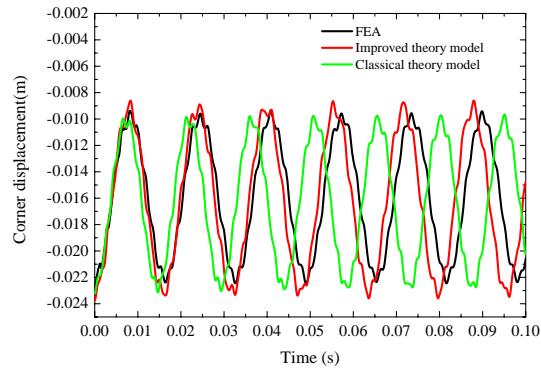
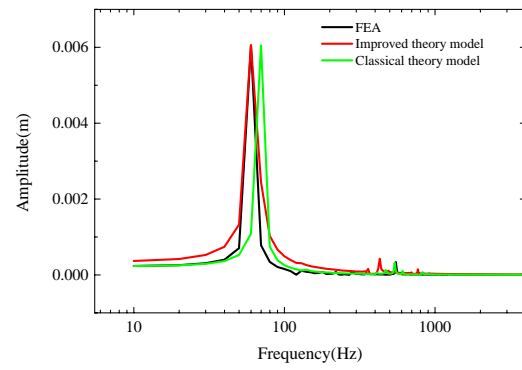


Figure 15: Load-displacement curve of $150\text{mm} \times 100\text{mm}$, $[0_{0.5\text{mm}}/90_{0.5\text{mm}}]_T$ plate mounted at central.



(a)



(b)

Figure 16: Dynamic response of the $150\text{mm} \times 150\text{mm}$, $[0_{0.25\text{mm}}/90_{0.25\text{mm}}]$ bi-stable plate. (a) Time series; (b) FFT.

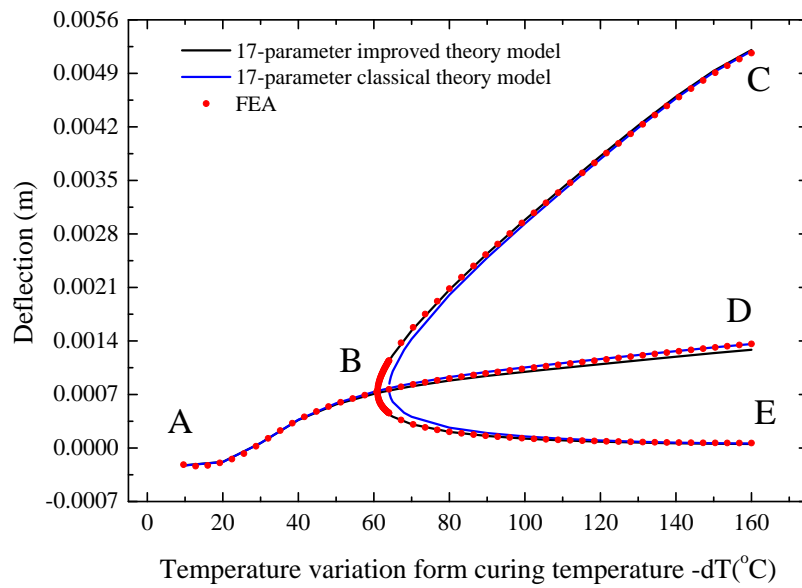


Figure 17: Out-of-plane deflections of middle points at the edges of $80\text{mm} \times 80\text{mm}$, $[0_{0.25\text{mm}}/90_{0.25\text{mm}}]_T$ plate with temperature dependent materials properties mounted at central.